The Astrophysical Journal, 746:101 (26pp), 2012 February 10 doi:10.1088/0004-637X/746/1/101

STELLAR DIAMETERS AND TEMPERATURES. I. MAIN-SEQUENCE A, F, AND G STARS

Tabetha S. Boyajian[1,6], Harold A. McAlister[1], Gerard van Belle[2], Douglas R. Gies[1], Theo A. ten Brummelaar[3], Kaspar von Braun[4], Chris Farrington[3], P. J. Goldfinger[3], David O'Brien[1], J. Robert Parks[1], Noel D. Richardson[1], Stephen Ridgway[5], Gail Schaefer[3], Laszlo Sturmann[3], Judit Sturmann[3], Yamina Touhami[1], Nils H. Turner[3], and Russel White[1]

[1] Center for High Angular Resolution Astronomy and Department of Physics and Astronomy, Georgia State University, Atlanta, GA 30302-4106, USA
[2] Lowell Observatory, Flagstaff, AZ 86001, USA
[3] The CHARA Array, Mount Wilson Observatory, Mount Wilson, CA 91023, USA
[4] NASA Exoplanet Science Institute, California Institute of Technology, MC 100-22, Pasadena, CA 91125, USA
[5] National Optical Astronomy Observatory, Tucson, AZ 85726-6732, USA
Received 2011 October 28; accepted 2011 December 14; published 2012 January 27

ABSTRACT

We have executed a survey of nearby, main-sequence A-, F-, and G-type stars with the CHARA Array, successfully measuring the angular diameters of forty-four stars with an average precision of ∼1.5%. We present new measures of the bolometric flux, which in turn leads to an empirical determination of the effective temperature for the stars observed. In addition, these CHARA-determined temperatures, radii, and luminosities are fit to Yonsei–Yale model isochrones to constrain the masses and ages of the stars. These results are compared to indirect estimates of these quantities obtained by collecting photometry of the stars and applying them to model atmospheres and evolutionary isochrones. We find that for most cases, the models overestimate the effective temperature by ∼1.5%–4% when compared to our directly measured values. The overestimated temperatures and underestimated radii in these works appear to cause an additional offset in the star's surface gravity measurements, which consequently yield higher masses and younger ages, in particular for stars with masses greater than $\sim 1.3\,M_{\odot}$. Additionally, we compare our measurements to a large sample of eclipsing binary stars, and excellent agreement is seen within both data sets. Finally, we present temperature relations with respect to $(B-V)$ and $(V-K)$ colors as well as spectral type, showing that calibration of effective temperatures with errors ∼1% is now possible from interferometric angular diameters of stars.

Key words: Hertzsprung–Russell and C–M diagrams – infrared: stars – stars: evolution – stars: fundamental parameters – stars: late-type – stars: solar-type – techniques: interferometric

Online-only material: color figures, machine-readable table

1. INTRODUCTION

The direct measurement of the stellar angular diameter is a valuable key in determining fundamental properties of a star, particularly the linear radius and effective temperature. These properties of a star provide the link between the theory of stellar structure and evolution to model atmospheres. For nearby, main-sequence stars, where we know their distances well, the angular diameters are difficult to measure due to their tiny sizes compared to their evolved counterparts. The high angular resolution obtained through long-baseline optical/infrared interferometry has enabled us to resolve the photospheric disks of such nearby stars.

Several decades ago, a survey carried out at the Narrabri Stellar Intensity Interferometer (NSII; Hanbury Brown et al. 1974a; Code et al. 1976) was conducted to measure the angular diameters of 32 stars. This survey extended from O- to F-type stars, 11 of which were roughly on the main sequence (luminosity class V or IV).[7] For several decades, luminosity class I, II, and III stars were observed with interferometers such as the Mark III and the Palomar Testbed Interferometer, but no main-sequence star earlier than A7 was measured (Davis 1997).

As an update, the CHARM2 Catalogue (Richichi et al. 2005) provides a compilation of stellar diameters by means of direct measurements by high angular resolution methods, as well as indirect estimates. The CHARM2 Catalogue includes all results as of 2004 July, a total of 8231 entries. Filtering out the entries to include only unique sources where direct measurements exist with errors in the angular diameter measurements of less than 5%, this number drops to 242, and only 24 of these reside on the main sequence (luminosity class V or IV).

In a recent work by Holmberg et al. (2008), they remark that measurements of the angular diameters of main-sequence F and G stars need to be better than 2%, yielding temperatures to 1%, in order for offsets in the color–temperature calibrations to be minimal. At that time, only nine stars met this criterion. This precision limit reiterates the target accuracy proposed by Blackwell et al. (1979) for the limits to the Infrared Flux Method that a good $T_{\rm EFF}$ determination goal should be 1% to match the best atomic data available for abundance determinations and $\log g$ estimates (Davis 1985; Booth 1997).

The long baselines of the CHARA Array are uniquely suited for observing diameters of main-sequence stars to great precision. In this paper, we present the angular diameters of 44 main-sequence A-, F-, and G-type stars measured with the CHARA Array, the most extensive interferometric survey of main-sequence stars to date. Details on the observing strategy and observations are in Section 2, and the results are presented

[6] Hubble Fellow.
[7] The average precision of these angular diameter determinations depended primarily on the brightness of the object and was ≈6.5% for the 32 stars measured.

and discussed in Section 3. In Section 3, we also discuss the consistency of our results compared to the recent work of van Belle & von Braun (2009), who used the Palomar Testbed Interferometer to observe a few dozen main-sequence stars, where 14 of these stars are common sources with this work. Section 4 introduces the fundamental stellar properties of linear radii, luminosities, and effective temperatures for the stars observed. In the discussion (Section 5), we use our data to derive empirical temperature relations to $(B-V)$ and $(V-K)$ colors and spectral type. We also present masses and ages for the sample obtained via isochrone fitting and masses computed by combining our radii with published values of surface gravities. Our results are compared to three surveys in the literature that have a large percentage of stars in common with our survey, as well as a large sample of non-interacting eclipsing binaries. We summarize in Section 6.

2. OBSERVATIONS WITH THE CHARA ARRAY

2.1. Instrument

The CHARA Array is an optical/infrared interferometric array located at Mount Wilson Observatory in the San Gabriel mountains of southern California (a detailed description of the instrument can be found in ten Brummelaar et al. 2005). Briefly, the CHARA Array consists of six, 1 m aperture telescopes in a Y-shaped configuration spread across the mountaintop of the Observatory. With the six telescopes, there are 15 available baseline combinations, ranging from 34 to 331 m, at a variety of position angle orientations ψ. The CHARA Array currently is the longest baseline operational optical/infrared interferometer in the world.

There are several beam combiners available for the CHARA Array, and for this project, the observations were made using the CHARA Classic beam combiner in two-telescope mode. CHARA Classic is a pupil-plane beam combiner, which is used in the K' band, empirically measured in Bowsher et al. (2010) to have a central wavelength of $\lambda_{K'} = 2.141 \pm 0.003\ \mu$m. Fringes are detected and recorded on the Near Infrared Observer (NIRO) camera, which is based upon an HgCdTe PICNIC Array readout at high speed. Nearly all (98.5%) of the observing for this work was performed remotely from Georgia State University's Cleon Arrington Remote Operations Center (AROC) in Atlanta, GA during the 2007, 2008, and 2009 observing seasons.

2.2. Target Selection

The main goal of this survey is to determine the angular diameters of a large number of stars to high precision. We limited the stars observed by selecting only those for which the predicted precision of the measured angular diameter will be better than 4%. The precision of a measurement of the stellar angular diameter depends on how far down the visibility curve one is able to sample. The expression of the uniform disk visibility function of a single star (Equation (1)) is dependent on B the projected baseline, θ the angular diameter of the star, and λ the wavelength of observation:

$$V = \frac{2J_1(x)}{x}, \quad (1)$$

where

$$x = \pi B \theta \lambda^{-1} \quad (2)$$

and J_1 is the first-order Bessel function. By knowing the λ and B utilized in a given observation, we can estimate the optimum resolution range resulting from the precision with which we can measure the object visibility. To ensure that we reach the precision goal of $\sigma\theta < 4\%$ for our observations, we find the approximate limiting resolution is $\theta \sim 0.65$ mas for K'. In reality, this number will vary (for example, see Baines et al. 2008), but its use to establish a first-order cutoff for a preliminary sample selection is appropriate.

Each star we chose to observe was then hand selected from a *Hipparcos* catalog query. This process was initiated from assumptions of the nominal linear size of a main-sequence star from Cox (2000) based on $B-V$ colors, in order to determine a maximum distance to be sampled for each spectral type before reaching the $\theta = 0.65$ mas resolution limit. Additionally, the luminosity class of the star was restricted by apparent V magnitudes to only admit roughly main-sequence stars (Cox 2000). The declination limit to this survey was restricted to targets above $-10°$ declination. All stars were easily within the magnitude limits for observing with the CHARA Array, with magnitudes ranging from $2.5 < V < 6.4$ and $1.6 < K < 4.4$.[8] Table 1 lists the names, coordinates, spectral types, magnitudes, metallicity [Fe/H], and *Hipparcos* distance of the stars observed.

2.3. Data Calibration

We follow the standard routine for interferometric observing where a calibrator star with known size is observed before and after every observation of a science object,[9] which enables us to remove the instrumental response of the system as well as effects from local seeing conditions. A description of the ideal calibrator and the propagation of errors to the true visibility measurements of the science star can be found in van Belle & van Belle (2005). The calibrator stars used in this work were initially selected from the getCal web interface[10] and were restricted by angular distance in the sky to the object, magnitude, and its estimated angular size. In most cases, the calibrator star was less than 6° from the object, and never lying further than ∼10°. The closeness of the object to the calibrator is crucial for quickly acquiring brackets, where under typical observing conditions, there is approximately 4–5 minutes between observations. The magnitudes of the calibrator stars were chosen from observability limits with our telescopes and instrument. Finally, the estimated angular size of the calibrator was the attribute that is most weighted in the calibrator searching process.

With CHARA's long baselines, unwanted biases may be introduced if the calibrator is resolved. If possible, calibrators were chosen to have a angular diameter less than 0.45 mas, following the example described in van Belle & van Belle (2005) for CHARA's maximum baseline of 331 m. In order to estimate the calibrator's angular size, $\theta_{\rm SED}$, a Kurucz model spectral energy distribution (SED) was fit to Johnson *UBV* (Mermilliod 1997), Strömgren *uvby* (Hauck & Mermilliod 1998), and Two Micron All Sky Survey (2MASS) *JHK* (Cutri et al. 2003) flux-calibrated photometry.[11] The calibrators used in this work are listed in Table 2. Table 2 also shows the calibrator Johnson, Strömgren, and 2MASS magnitudes, and $\theta_{\rm SED}$ fit for each star.

[8] Very conservative limits for observing with the CHARA Classic beam combiner require $V < 10$ mag and $K < 7$ mag.

[9] This sequence of calibrator–object–calibrator is called a "bracket."

[10] http://nexsciweb.ipac.caltech.edu/gcWeb/gcWeb.jsp

[11] Transformations from *UBV*, *uvby*, and *JHK* magnitudes to flux were made using the relations described in Colina et al. (1996), Gray (1998), and Cohen et al. (2003), respectively.

Table 1
Target Sample of A, F, and G Dwarfs

HD	HR	HIP	Other Name[a]	R.A. (hh mm ss.xx)	Decl. (dd mm ss)	Spectral Type[b]	Spectral Type[c]	V (mag)	K (mag)	$(B-V)$ (mag)	[Fe/H][d]	$\pi \pm \sigma$[e] (mas)
4614	219	3821	24 η Cas A	00 49 06.29	57 48 54.67	F9V	G0V	3.46	2.05	0.587	−0.30	168.01 ± 0.48
5015	244	4151	GJ 41	00 53 04.20	61 07 26.29	F8V	F8V	4.80	3.54	0.540	0.00	53.35 ± 0.33
6582	321	5336	34 μ Cas A	01 08 16.39	54 55 13.22	G5Vb	G5Vp	5.17	3.36	0.704	−0.83	132.40 ± 0.60
10780	511	8362	GJ 75	01 47 44.84	63 51 09.00	G9V	K0V	5.63	3.84	0.804	0.05	99.34 ± 0.53
16895	799	12777	13 θ Per A	02 44 11.99	49 13 42.41	F7V	F7V	4.10	2.78	0.514	−0.12	89.88 ± 0.23
19373	937	14632	ι Per	03 09 04.02	49 36 47.80	G0IV-V	G0V	4.05	2.70	0.595	0.09	94.87 ± 0.23
20630	996	15457	κ Cet	03 19 21.70	03 22 12.71	G5V	G5Vvar	4.84	3.34	0.681	0.00	109.39 ± 0.27
22484	1101	16852	10 Tau	03 36 52.38	00 24 05.98	F9IV-V	F9V	4.29	2.93	0.575	−0.09	71.60 ± 0.54
30652	1543	22449	1 π^3 Ori	04 49 50.41	06 57 40.59	F6IV-V	F6V	3.19	2.07	0.484	−0.03	123.94 ± 0.17
34411	1729	24813	15 λ Aur	05 19 08.47	40 05 56.59	G1V	G0V	4.69	3.24	0.630	0.05	79.18 ± 0.28
39587	2047	27913	54 χ^1 Ori	05 54 22.98	20 16 34.23	G0IV-V	G0V	4.39	2.97	0.594	−0.16	115.42 ± 0.27
48737	2484	32362	31 ξ Gem	06 45 17.37	12 53 44.13	F5IV-V	F5IV	3.35	2.30	0.443	0.01	55.55 ± 0.19
56537	2763	35350	54 λ Gem	07 18 05.58	16 32 25.38	···	A3V	3.58	3.27	0.106	···	32.36 ± 0.22
58946	2852	36366	62 ρ Gem	07 29 06.72	31 47 04.38	···	F0V	4.16	3.32	0.320	−0.31	55.41 ± 0.25
81937	3757	46733	23 h UMa	09 31 31.71	63 03 42.70	···	F0IV	3.65	2.82	0.360	0.06	41.99 ± 0.16
82328	3775	46853	25 θ UMa	09 32 51.43	51 40 38.28	F5.5IV-V	F6IV	3.17	2.02	0.475	−0.12	74.18 ± 0.13
82885	3815	47080	11 LMi	09 35 39.50	35 48 36.48	G8+V	G8IV-V	5.40	3.70	0.770	0.06	87.96 ± 0.32
86728	3951	49081	20 LMi	10 01 00.66	31 55 25.22	G4V	G3V	5.37	3.82	0.676	0.20	66.47 ± 0.32
90839	4112	51459	36 UMa	10 30 37.58	55 58 49.93	F8V	F8V	4.82	3.54	0.541	−0.16	78.26 ± 0.29
95418	4295	53910	48 β UMa	11 01 50.48	56 22 56.74	A1IV	A1V	2.34	2.35	0.033	0.06	40.89 ± 0.16
97603	4357	54872	68 δ Leo	11 14 06.50	20 31 25.38	A5IV(n)	A4V	2.56	2.26	0.128	0.00	55.82 ± 0.25
101501	4496	56997	61 UMa	11 41 03.02	34 12 05.89	G8V	G8V	5.31	3.53	0.723	−0.12	104.03 ± 0.26
102870	4540	57757	5 β Vir	11 50 41.72	01 45 52.98	F8.5IV-V	F8V	3.59	2.33	0.518	0.11	91.50 ± 0.22
103095	4550	57939	CF UMa	11 52 58.77	37 43 07.24	K1V	G8Vp	6.42	4.38	0.754	−1.36	109.98 ± 0.41
109358	4785	61317	8 β CVn	12 33 44.55	41 21 26.93	G0V	G0V	4.24	2.72	0.588	−0.30	118.49 ± 0.20
114710	4983	64394	43 β Com	13 11 52.39	27 52 41.46	G0V	G0V	4.23	2.90	0.572	−0.06	109.53 ± 0.17
118098	5107	66249	79 ζ Vir	13 34 41.59	−00 35 44.95	A2Van	A3V	3.38	3.11	0.114	−0.02	44.01 ± 0.19
126660	5404	70497	23 θ Boo	14 25 11.80	51 51 02.68	F7V	F7V	4.04	2.78	0.497	−0.14	68.83 ± 0.14
128167	5447	71284	28 σ Boo	14 34 40.82	29 44 42.47	F4VkF2mF1	F3V	4.47	3.52	0.364	−0.36	63.16 ± 0.26
131156	5544	72659	37 ξ Boo	14 51 23.38	19 06 01.66	G7V	G8V	4.54	2.96	0.720	−0.33	149.03 ± 0.48
141795	5892	77622	37 ϵ Ser	15 50 48.97	04 28 39.83	kA2hA5mA7V	A2m	3.71	3.43	0.147	···	46.28 ± 0.19
142860	5933	78072	41 γ Ser	15 56 27.18	15 39 41.82	F6V	F6V	3.85	2.66	0.478	−0.19	88.85 ± 0.18
146233	6060	79672	18 Sco	16 15 37.27	−08 22 09.99	G2V	G1V	5.49	3.55	0.652	−0.02	71.93 ± 0.37
162003	6636	86614	31 ψ Dra	17 41 56.36	72 08 55.84	F5IV-V	F5IV-V	4.57	3.43	0.434	−0.17	43.79 ± 0.45
164259	6710	88175	57 ζ Ser	18 00 29.01	−03 41 24.97	F2V	F3V	4.62	3.66	0.390	−0.14	42.44 ± 0.33
173667	7061	92043	110 Her	18 45 39.73	20 32 46.71	F5.5IV-V	F6V	4.19	2.89	0.483	−0.15	52.06 ± 0.24
177724	7235	93747	17 ζ Aql	19 05 24.61	13 51 48.52	A0IV-Vnn	A0Vn	2.99	2.92	0.014	−0.68	39.27 ± 0.17
182572	7373	95447	31 b Aql	19 24 58.20	11 56 39.90	···	G8IV	5.17	3.53	0.761	0.33	65.89 ± 0.26
185144	7462	96100	61 σ Dra	19 32 21.59	69 39 40.23	G9V	K0V	4.67	2.78	0.786	−0.24	173.77 ± 0.18
185395	7469	96441	13 θ Cyg	19 36 26.54	50 13 15.97	F3+V	F4V	4.49	3.52	0.395	−0.04	54.55 ± 0.15
210418	8450	109427	26 θ Peg	22 10 11.99	06 11 52.31	···	A2V	3.52	3.22	0.086	−0.38	35.34 ± 0.85
213558	8585	111169	7 α Lac	22 31 17.50	50 16 56.97	···	A1V	3.76	3.75	0.031	···	31.80 ± 0.12
215648	8665	112447	46 ξ Peg	22 46 41.58	12 10 22.40	F6V	F7V	4.20	2.87	0.502	−0.24	61.37 ± 0.20
222368	8969	116771	17 ι Psc	23 39 57.04	05 37 34.65	F7V	F7V	4.13	2.89	0.507	−0.08	72.91 ± 0.15

Notes.
[a] Bayer-Flamsteed or GJ (Kostjuk 2004).
[b] Gray et al. (2001, 2003).
[c] *SIMBAD* (Wenger et al. 2000).
[d] Holmberg et al. (2007), when available. For stars without metallicity estimates from Holmberg et al. (2007), the [M/H] values from Gray et al. (2003, 2006; HD 82885, HD 97603, HD 118098, HD 131156, HD 177724, HD 210418), and Takeda et al. (2005; HD 182572) are used. Stars with no metallicity measurements are HD 56537, HD 141795, and HD 213558.
[e] van Leeuwen (2007).

The last column lists the science object(s) observed with that calibrator.

Two-thirds of the calibrators used meet the $\theta_{\rm SED} < 0.45$ mas criteria.[12] In many cases, the science stars were observed with more than one calibrator, on more than one occasion, in order to reduce the likelihood of biases being introduced (for example, see HD 30652; Table 3). In some instances, we were not so fortunate to observe stars with multiple calibrators having the ideal angular size of $\theta_{\rm SED} < 0.45$ mas. For instance, the stars HD 5015, HD 6582, and HD 10780 were observed with only one calibrator, HD 6210 ($\theta_{\rm SED} = 0.519$ mas). However, we note that the observations of the star HD 4614 were also obtained with this calibrator as well as two additional calibrators, one of which meets the ideal criterion for being completely unresolved (HD 9407, $\theta_{\rm SED} = 0.430$ mas). We find that all the calibrated data sets for HD 4614 agree flawlessly in the final diameter fits.

[12] All have $\theta_{\rm SED} < 0.66$ mas, with a mean angular diameter error of 4.4%.

Table 2
Calibrators Observed

Calibrator HD	V (mag)	$B-V$ (mag)	$U-B$ (mag)	v (mag)	$b-y$ (mag)	$m1$ (mag)	$c1$ (mag)	J (mag)	H (mag)	K (mag)	$\theta_{\rm SED} \pm \sigma$ (mas)	Target (s) HD
71	6.990	1.187	...	...	...	...	...	5.193	4.459	4.214	0.682 ± 0.024	4614
6210	5.838	0.547	0.110	5.800	0.356	0.183	0.475	4.755	4.794	4.445	0.519 ± 0.012	4614, 5015, 6582, 10780
9407	6.530	0.684	0.236	...	...	...	...	5.296	4.941	4.888	0.430 ± 0.017	4614
20675	5.932	0.441	−0.015	5.950	0.293	0.167	0.495	5.274	4.922	4.875	0.415 ± 0.012	16895, 19373
21790	4.727	−0.093	−0.260	4.738	−0.036	0.107	0.833	5.282	4.960	4.886	0.308 ± 0.009	20630, 22484
22879	6.689	0.540	−0.086	6.693	0.365	0.126	0.272	5.588	5.301	5.179	0.342 ± 0.021	20630, 22484
28355	5.025	0.218	0.120	5.023	0.115	0.225	0.909	4.793	4.656	4.534	0.425 ± 0.030	30652
30739	4.355	0.009	−0.016	4.370	0.010	0.153	1.107	3.825	4.208	4.166	0.461 ± 0.018	30652
31295	4.644	0.085	0.095	4.661	0.044	0.178	1.007	4.846	4.517	4.416	0.439 ± 0.043	30652
34904	5.540	0.120	0.120	5.540	0.084	0.163	1.101	5.144	5.124	5.112	0.345 ± 0.013	34411
38558	5.527	0.274	0.249	5.400	0.196	0.148	1.176	4.944	4.746	4.483	0.422 ± 0.008	39587
42807	6.442	0.660	0.160	6.440	0.415	0.228	0.292	5.253	5.010	4.849	0.429 ± 0.016	48737
43042	5.201	0.434	−0.011	5.207	0.291	0.166	0.443	4.008	3.827	4.129	0.591 ± 0.030	39587
43795	7.640	0.958	...	7.645	0.593	0.293	0.483	5.940	5.522	5.409	0.376 ± 0.008	48682
50277	5.765	0.265	0.089	5.764	0.154	0.184	0.872	5.308	5.232	5.088	0.346 ± 0.011	48737
50973	4.897	0.029	0.053	4.917	0.013	0.159	1.107	5.055	4.941	4.793	0.361 ± 0.026	48682
58551	6.544	0.460	0.000	6.539	0.322	0.129	0.355	5.534	5.380	5.245	0.357 ± 0.009	56537
59037	5.011	0.112	0.119	5.084	0.063	0.201	1.015	4.818	4.793	4.744	0.389 ± 0.018	58946
65583	6.999	0.713	0.181	6.975	0.450	0.232	0.231	5.539	5.170	5.095	0.406 ± 0.033	58946
79439	4.832	0.186	0.087	0.113	0.196	0.892	2.833	4.481	4.353	4.291	0.482 ± 0.035	82328
80290	6.160	0.420	−0.110	6.132	0.300	0.139	0.392	5.219	5.067	4.972	0.385 ± 0.016	82328
83951	6.140	0.360	0.000	6.000	0.244	0.162	0.594	5.355	5.246	5.169	0.360 ± 0.006	82885, 86728
87141	5.749	0.476	0.043	5.700	0.318	0.169	0.478	4.987	4.730	4.503	0.476 ± 0.022	81937, 82328, 95418
88986	6.460	0.600	0.160	6.440	0.397	0.209	0.363	5.247	4.946	4.884	0.432 ± 0.013	82885, 86728
89389	6.450	0.540	0.080	0.369	0.181	0.370	2.602	5.340	5.091	5.020	0.398 ± 0.013	81937, 82328, 90839, 95418
91480	5.159	0.335	−0.020	5.140	0.228	0.159	0.574	4.922	4.688	4.334	0.518 ± 0.014	81937, 90839, 95418
99285	5.610	0.345	−0.017	5.640	0.251	0.154	0.595	4.815	4.723	4.624	0.456 ± 0.017	97603
99984	5.964	0.493	−0.025	5.800	0.340	0.148	0.429	4.900	4.657	4.591	0.483 ± 0.020	103095
102124	4.838	0.176	0.091	4.858	0.090	0.196	0.926	4.634	4.542	4.409	0.466 ± 0.022	102870
102634	6.145	0.520	0.069	6.153	0.329	0.176	0.439	5.212	5.081	4.921	0.404 ± 0.010	102870
103799	6.622	0.469	−0.026	0.326	0.139	0.422	2.618	5.594	5.386	5.338	0.343 ± 0.013	101501, 103095, 109358
110897	5.956	0.548	−0.044	5.958	0.374	0.147	0.284	5.173	4.667	4.465	0.492 ± 0.022	109358
114093	6.830	0.910	0.000	...	...	...	...	5.115	4.739	4.564	0.572 ± 0.014	114710
116831	5.956	0.187	0.125	5.973	0.095	0.206	0.972	5.668	5.577	5.531	0.278 ± 0.020	118098
120066	6.329	0.621	0.151	6.329	0.399	0.188	0.397	5.212	4.997	4.851	0.428 ± 0.013	118098
128093	6.332	0.397	−0.022	6.200	0.300	0.131	0.476	5.460	5.287	5.222	0.351 ± 0.011	128167
129153	5.915	0.218	0.045	0.131	0.206	0.813	2.816	5.447	5.402	5.365	0.309 ± 0.010	131156
132254	5.639	0.496	−0.003	5.600	0.338	0.174	0.410	4.685	4.464	4.408	0.520 ± 0.015	126660
135101	6.689	0.680	0.260	6.685	0.433	0.220	0.368	5.403	5.090	5.030	0.409 ± 0.014	131156
139225	5.950	0.280	0.020	5.800	0.222	0.160	0.681	5.175	5.099	5.023	0.380 ± 0.122	142860
140775	5.571	0.035	0.059	5.568	0.024	0.150	1.107	5.466	5.463	5.428	0.275 ± 0.013	141795
145607	5.420	0.120	0.120	5.443	0.059	0.172	1.083	5.170	5.307	5.052	0.325 ± 0.020	146233
150177	6.390	0.490	−0.100	6.333	0.334	0.119	0.395	5.353	5.064	4.977	0.391 ± 0.019	146233
154099	6.300	0.240	0.110	6.308	0.158	0.180	0.944	5.706	5.633	5.604	0.283 ± 0.005	162003
158352	5.418	0.227	0.094	5.420	0.148	0.183	0.923	4.813	4.883	4.805	0.407 ± 0.013	164259
162004	5.808	0.531	0.032	5.780	0.346	0.160	0.379	5.001	4.590	4.527	0.498 ± 0.015	162003
167564	6.350	0.200	0.150	6.354	0.123	0.158	1.148	5.891	5.791	5.750	0.259 ± 0.004	165259
174897	6.550	1.050	0.850	...	...	...	...	4.797	4.384	4.096	0.652 ± 0.038	182572
176303	5.239	0.530	0.066	5.267	0.356	0.168	0.452	4.324	4.039	3.930	0.659 ± 0.016	173667, 177724, 182572
180317	5.640	0.110	0.000	5.600	0.068	0.184	1.072	5.330	5.381	5.302	0.309 ± 0.007	173667, 177724
183534	5.750	0.000	−0.020	5.750	−0.003	0.157	1.023	5.632	5.690	5.674	0.241 ± 0.012	185395
191195	5.826	0.418	−0.030	5.817	0.284	0.153	0.506	5.239	4.834	4.766	0.432 ± 0.014	185395
193664	5.919	0.585	0.058	5.922	0.382	0.180	0.323	4.879	4.690	4.451	0.494 ± 0.019	185144
204485	5.797	0.304	0.009	5.700	0.200	0.198	0.648	5.156	5.020	4.955	0.381 ± 0.011	201091, 201092
210715	5.393	0.154	0.069	5.400	0.076	0.200	0.967	5.013	5.016	4.959	0.366 ± 0.015	213558
211976	6.178	0.450	−0.052	6.183	0.300	0.148	0.423	5.323	5.160	5.050	0.373 ± 0.013	210418, 215648
214923	3.406	−0.086	−0.217	3.406	−0.035	0.113	0.868	3.538	3.527	3.566	0.611 ± 0.029	215648
216735	4.906	−0.002	0.003	4.915	−0.006	0.159	1.083	5.222	5.012	4.840	0.321 ± 0.022	215648, 222368
218470	5.680	0.417	−0.039	5.687	0.290	0.146	0.486	4.819	4.670	4.649	0.462 ± 0.014	213558
222603	4.502	0.202	0.078	4.500	0.105	0.203	0.891	4.372	4.204	4.064	0.577 ± 0.032	222368
225003	5.704	0.329	−0.007	5.699	0.209	0.155	0.645	5.077	5.008	4.910	0.386 ± 0.017	222368

Notes. Johnson *UBV* (Mermilliod 1997), Stromgren *uvby* (Hauck & Mermilliod 1998), and 2MASS *JHK* (Cutri et al. 2003) magnitudes for the calibrator stars. Refer to Section 2.3 for details.

Table 3
Observation Log

Object HD	UT Date (yyyy/mm/dd)	Baseline	No. of Brackets	Calibrator HD
4614	2007/06/29	W1/E1	2	6210
	2007/06/30	W1/E1	5	6210
	2007/07/01	W1/E1	3	6210
	2007/07/18	S1/E1	3	6210
	2007/07/19	S1/E1	3	6210
	2007/11/16	S1/E1	4	6210
	2008/10/02	W1/E1	4	6210, 9407
	2009/11/21	S1/E1	3	71
5015	2007/10/10	W1/E1	10	6210
	2007/11/03	W1/E1	7	6210
	2007/11/17	S1/E1	8	6210
6582	2007/07/01	W1/E1	3	6210
	2007/07/17	S1/E1	6	6210
	2007/07/18	S1/E1	8	6210
	2007/09/08	S1/E1	10	6210
10780	2007/06/29	W1/E1	2	6210
	2007/07/19	S1/E1	10	6210
	2007/10/10	W1/E1	10	6210
16895	2007/09/08	S1/E1	7	20675
	2007/11/03	W1/E1	8	20675
	2007/12/24	S1/E1	6	20675
19373	2007/01/25	S1/E1	8	20675
	2007/08/28	W1/S1	2	20675
	2007/09/08	S1/E1	10	20675
	2007/11/04	W1/E1	6	20675
20630	2007/09/09	S1/E1	9	21790
	2008/10/01	S1/E1	4	22879
	2008/11/17	S1/E1	5	22879
	2008/11/18	S1/E1	5	21790, 22879
22484	2006/12/05	S1/E1	2	21790
	2006/12/07	S1/E1	3	21790
	2007/09/09	S1/E1	8	21790
	2008/10/01	S1/E1	6	22879
	2008/10/02	W1/E1	4	22879
30652	2007/11/05	S1/E1	16	30739
	2008/10/01	S1/E1	10	28355, 31295
	2008/10/02	W1/E1	3	31295
34411	2007/01/26	S1/E1	5	34904
	2007/11/03	W1/E1	8	34904
	2007/11/15	S1/E1	4	34904
	2007/11/17	S1/E1	7	34904
39587	2006/12/07	S1/E1	3	38558
	2007/03/06	S1/E1	8	38558
	2008/11/18	S1/E1	11	38558, 43042
48737	2006/12/07	S1/E1	4	50277
	2008/11/17	S1/E1	12	42807, 50277
	2008/11/18	S1/E1	11	42807, 50277
56537	2007/02/21	S1/E1	1	58551
	2007/02/25	S1/E1	7	58551
	2007/03/11	S1/E1	6	58551
	2007/11/04	S1/E1	5	58551
	2007/12/23	S1/E1	5	58551
58946	2007/01/25	S1/E1	6	65583
	2007/11/16	S1/E1	7	59037
	2007/11/17	S1/E1	7	59037
81937	2007/11/29	S2/E2	9	91480
	2009/11/20	S1/E1	12	87141, 89389, 91480
	2009/11/21	S1/E1	4	87141
	2009/11/22	S1/E1	2	91480

Table 3
(Cotninued)

Object HD	UT Date (yyyy/mm/dd)	Baseline	No. of Brackets	Calibrator HD
82328	2007/11/02	W2/E2	9	87141
	2009/11/20	S1/E1	7	79439, 80290, 89389
	2009/11/22	S1/E1	3	79439
82885	2007/02/03	S1/E1	2	83951
	2007/11/03	W1/E1	7	83951
	2007/11/07	S1/E1	9	83951
	2007/12/24	S1/E1	5	83951
	2009/11/21	S1/E1	3	88986
86728	2007/11/15	S1/E1	10	83951
	2007/11/16	S1/E1	2	83951
	2007/12/24	S1/E1	6	83951
	2008/11/16	S1/E1	10	83951, 88986
	2009/11/21	S1/E1	4	88986
90839	2007/11/16	S1/E1	10	89389
	2008/04/17	W1/S1	5	89389, 91480
95418	2007/04/04	S1/E1	7	91480
	2007/11/07	S1/E1	6	91480
	2008/04/17	W1/S1	5	89389, 91480
	2009/11/21	S1/E1	3	87141
	2009/11/22	S1/E1	4	91480
97603	2007/02/21	S1/E1	10	99285
	2007/03/10	S1/E1	2	99285
	2007/03/11	S1/E1	5	99285
101501	2007/11/15	S1/E1	7	103799
	2007/12/24	S1/E1	3	103799
102870	2007/03/09	S1/E1	6	102124
	2007/12/23	S1/E1	4	102124
	2008/04/19	W1/S1	8	102124
	2008/04/22	S1/E1	9	102124
	2008/04/23	S1/E1	7	102634
103095	2007/11/16	S1/E1	7	103799
	2007/12/24	S1/E1	10	103799
109358	2007/05/26	S1/E2	3	110897
	2008/04/18	W1/S1	5	103799, 110897
114710	2008/04/21	W1/S1	10	114093
	2008/06/27	S1/E1	6	114093
118098	2007/03/10	S1/E1	6	120066
	2007/03/30	S1/E1	5	120066
	2007/12/23	S1/E1	2	120066
	2010/04/10	S1/E1	4	116831, 120066
126660	2007/05/24	W1/S1	5	132254
	2007/07/16	S1/E1	6	132254
	2008/07/25	S1/E1	4	132254
128167	2008/06/28	S1/E1	5	128093
	2008/07/06	S1/E1	12	128093
	2008/07/24	S1/E2	10	128093
131156	2007/03/12	S1/E1	5	135101
	2008/04/18	W1/S1	5	135101, 129153
	2008/04/19	W1/S1	6	135101
	2008/06/27	S1/E1	9	135101, 129153
141795	2008/07/22	S1/E1	8	140775
142860	2007/07/20	S1/E1	3	139225
	2007/07/21	S1/E1	6	139225
	2008/04/21	W1/S1	10	139225
146233	2008/04/19	W1/S1	11	145607, 150177
	2008/04/21	W1/S1	6	145607, 150177
	2008/04/22	S1/E1	9	145607, 150177
	2008/04/23	S1/E1	6	145607, 150177
	2008/05/16	W1/E2	4	150177

Table 3
(Cotninued)

Object HD	UT Date (yyyy/mm/dd)	Baseline	No. of Brackets	Calibrator HD
162003	2007/07/17	S1/E1	8	154099
	2007/07/18	S1/E1	2	162004
	2007/10/10	W1/E1	6	162004
	2007/11/17	S1/E1	4	162004
	2008/06/26	S1/E1	5	162004
164259	2008/04/22	S1/E1	6	167564, 158352
	2008/04/23	S1/E1	3	158352
	2008/06/20	W1/S1	3	158352
	2008/06/28	S1/E1	5	158352
	2008/07/27	W1/S1	6	158352
173667	2007/07/20	S1/E1	3	180317
	2007/07/21	S1/E1	9	176303
	2008/04/21	W1/S1	3	176303
	2008/06/28	S1/E1	8	176303
	2008/07/07	W1/S1	1	176303
	2008/07/21	W1/S1	1	176303
	2008/07/22	S1/E1	6	176303
	2008/07/23	W1/E1	6	176303
177724	2008/06/28	S1/E1	10	176303
	2008/07/07	W1/S1	5	176303
	2008/07/21	W1/S1	4	176303
	2008/07/22	S1/E1	6	176303
	2008/07/23	W1/E1	6	176303
	2008/10/01	S1/E1	4	176303
182572	2007/07/21	S1/E1	6	174897
	2007/09/09	S1/E1	10	174897
	2008/07/22	S1/E1	5	174897
	2008/07/24	S1/E2	5	174897
	2008/09/30	S1/E1	7	176303
185144	2007/05/24	W1/S1	3	193664
	2007/05/25	W1/S1	4	193664
	2007/06/28	W1/E1	1	193664
	2007/06/29	W1/E1	4	193664
	2007/06/30	W1/E1	1	193664
	2007/07/01	W1/E1	2	193664
185395	2007/05/26	S1/E2	3	183534
	2007/07/19	S1/E1	11	191195
	2007/11/02	W1/E2	5	191195
	2008/07/25	S1/E1	8	191195
201091	2007/06/30	W1/E1	3	204485
201092	2007/06/30	W1/E1	3	204485
210418	2008/06/28	S1/E1	6	211976
	2008/07/22	S1/E1	9	211976
	2008/07/24	S1/E2	4	211976
	2008/10/01	S1/E1	3	211976
213558	2007/09/08	S1/E1	7	218470
	2007/10/10	W1/E1	10	210715
	2007/12/24	S1/E1	6	218470
	2008/07/21	S1/E1	5	218470
215648	2007/07/16	S1/E1	4	211976
	2007/07/21	S1/E1	14	214923
	2008/07/24	S1/E2	5	214923
	2008/09/30	S1/E1	4	211976
	2008/10/01	S1/E1	8	211976, 216735
222368	2006/12/07	S1/E1	4	222603
	2007/07/20	S1/E1	11	222603
	2007/09/09	S1/E1	5	222603
	2008/09/30	S1/E1	10	222603, 225003
	2008/10/01	S1/E1	8	216735

Note. Refer to Section 2.3 for details.

Table 4
CHARA Baseline Configurations

Telescope Pair	B (m)	ψ (°)
W2/E2	156.28	63.3
S2/E2	248.13	17.7
W1/E2	251.34	77.6
W1/S1	278.50	320.9
S1/E2	278.77	14.5
W1/E1	313.54	253.2
S1/E1	330.67	22.1

Thus, using the slightly resolved calibrator star HD 6210 is not a cause of concern. Only four stars, HD 97603, HD 185144, HD 126660, and HD 114710 have observations with only one calibrator with 0.45 mas $< \theta_{\rm SED} <$ 0.57 mas, but consistency in the calibration process seen with stars observed with more than one calibrator (such as HD 4614) provides assurance that this issue is not a problematic one. Additionally, the maximum CHARA baseline of 331 m was never reached for a significant amount of these observations, thus pushing the theorized ideal maximum angular size for the calibrator to larger sizes.

The observing log is shown in Table 3 and lists the identifications of the 44 stars observed in this work (Column 1), UT date (Column 2), CHARA baseline (Column 3), number of brackets (Column 4), and the calibrator(s) used on that date (Column 5). The specifics of the CHARA baseline configurations are displayed in Table 4. We include the observations of HD 6582, HD 10780, and HD 185144 here for completeness, because they are an original part of this survey, but their results have been previously presented in Boyajian et al. (2008).

3. ANGULAR DIAMETERS

Angular diameters for each star were determined by fitting our interferometric measurements to the visibility curve for a single star's uniform disk $\theta_{\rm UD}$ and limb-darkened $\theta_{\rm LD}$ (Hanbury Brown et al. 1974b) angular diameters from the calibrated visibilities by χ^2 minimization (Markwardt 2009). To account for limb darkening, we use the K-band limb-darkening coefficients computed in Claret (2000). Limb-darkening corrections are at the 2% level in the infrared, and for these types of stars the uncertainty of this correction is at most a tenth of a percent, well within our error budget.

We find that in most cases the value of the reduced χ^2 is less than 1.0, meaning that we have overestimated the errors on the calculated visibilities for the star. The results presented here adjust those error estimates to assume a reduced $\chi^2 = 1$ to compensate for the uncertainty in the visibility error estimates (Berger et al. 2006). Table 5 presents the total number of observations, reduced χ^2, uniform disk diameter $\theta_{\rm UD}$, limb-darkening coefficient μ_K, and limb-darkened diameter $\theta_{\rm LD}$ for each star. The resulting fit for each star is plotted in Figure 1. Overall, we successfully measure the angular diameters of 8 A stars, 20 F stars, and 16 G stars, with an average precision of ~1.5%.

3.1. Notes on Individual Star Groups

3.1.1. A Stars

The results for the A-type stars (eight total) are special cases. A-type stars are approaching the range at which stars begin to be seen with the highest rotational velocities (B-type stars),

Table 5
Angular Diameters

Star HD	No. of Observations	Reduced χ^2	$\theta_{UD} \pm \sigma$ (mas)	μ_K	$\theta_{LD} \pm \sigma$ (mas)
4614	27	1.43	1.578 ± 0.004	0.280	1.623 ± 0.004
5015	22	0.45	0.846 ± 0.010	0.270	0.865 ± 0.010
6582	26	0.96	0.947 ± 0.009	0.320	0.972 ± 0.009
10780	22	0.78	0.744 ± 0.018	0.310	0.763 ± 0.019
16895	21	1.02	1.078 ± 0.008	0.270	1.103 ± 0.009
19373	22	0.90	1.217 ± 0.007	0.270	1.246 ± 0.008
20630	21	1.15	0.914 ± 0.024	0.290	0.936 ± 0.025
22484	23	1.05	1.056 ± 0.014	0.280	1.081 ± 0.014
30652	34	0.60	1.488 ± 0.004	0.260	1.526 ± 0.004
34411	18	1.07	0.958 ± 0.015	0.290	0.981 ± 0.015
39587	17	0.33	1.027 ± 0.009	0.280	1.051 ± 0.009
48737	24	1.49	1.369 ± 0.009	0.180	1.401 ± 0.009
56537	20	0.52	0.824 ± 0.013	0.250	0.835 ± 0.013
58946	15	0.51	0.837 ± 0.013	0.230	0.853 ± 0.014
81937	18	0.34	1.113 ± 0.009	0.260	1.133 ± 0.009
82328	19	0.54	1.591 ± 0.005	0.320	1.632 ± 0.005
82885	25	0.45	0.800 ± 0.012	0.290	0.821 ± 0.013
86728	28	0.62	0.753 ± 0.012	0.260	0.771 ± 0.012
90839	19	0.38	0.778 ± 0.014	0.180	0.794 ± 0.014
95418	29	1.41	1.133 ± 0.014	0.210	1.149 ± 0.014
97603	16	1.59	1.304 ± 0.008	0.310	1.328 ± 0.009
101501	10	0.22	0.887 ± 0.009	0.270	0.910 ± 0.009
102870	32	0.54	1.396 ± 0.006	0.320	1.431 ± 0.006
103095	16	0.08	0.679 ± 0.005	0.280	0.696 ± 0.005
109358	12	1.97	1.209 ± 0.030	0.280	1.238 ± 0.030
114710	16	0.40	1.100 ± 0.011	0.180	1.127 ± 0.011
118098	15	0.17	0.840 ± 0.009	0.260	0.852 ± 0.009
126660	15	0.43	1.086 ± 0.007	0.250	1.109 ± 0.007
128167	26	0.40	0.824 ± 0.013	0.320	0.841 ± 0.013
131156	30	1.92	1.163 ± 0.014	0.210	1.196 ± 0.014
141795	8	0.10	0.756 ± 0.017	0.260	0.768 ± 0.017
142860	19	0.11	1.191 ± 0.005	0.290	1.217 ± 0.005
146233	25	0.46	0.763 ± 0.017	0.250	0.780 ± 0.017
162003	25	2.23	0.930 ± 0.025	0.240	0.949 ± 0.026
164259	19	0.56	0.761 ± 0.027	0.250	0.775 ± 0.027
173667	42	1.06	0.979 ± 0.006	0.170	1.000 ± 0.006
177724	31	1.05	0.883 ± 0.016	0.320	0.895 ± 0.017
182572	33	1.91	0.823 ± 0.025	0.320	0.845 ± 0.025
185144	15	1.00	1.219 ± 0.011	0.240	1.254 ± 0.012
185395	25	0.86	0.845 ± 0.015	0.200	0.861 ± 0.015
210418	20	0.32	0.849 ± 0.017	0.180	0.862 ± 0.018
213558	27	0.84	0.625 ± 0.021	0.260	0.634 ± 0.022
215648	34	1.06	1.068 ± 0.008	0.260	1.091 ± 0.008
222368	36	0.90	1.059 ± 0.009	0.260	1.082 ± 0.009

Note. Refer to Section 3 for details.

resulting in oblate shapes and apparent gravity darkening due to their rapid rotation (for example, see Zhao et al. 2009). This oblateness factor depends on the star's θ_{LD}, rotational velocity $v \sin i$, and mass (see Equation (5) in Absil et al. 2008). The most extreme case that we observed is HD 177724, which is among one of the fastest rotating A stars, with a rotational velocity $v \sin i = 317$ km s^{-1} (Royer et al. 2006), which leads to a predicted apparent oblateness of 1.307 (Absil et al. 2008). Using all measurements and assuming the object to be round, we present the mean diameter for HD 177724 of $\theta_{LD} = 0.897 \pm 0.017$ mas (Table 5). This value is in excellent agreement with the predicted mean angular diameter from Absil et al. (2008) of $\theta = 0.880 \pm 0.018$ mas. The rotational velocity for all of the A stars in this project (except for HD 141795; $v \sin i = 47$ km s^{-1}) are fairly high (HD 56537 = 154 km s^{-1}, HD 97603 = 180 km s^{-1}, HD 118098 = 222 km s^{-1}, HD 210418 = 144 km s^{-1}, and HD 213558 = 128 km s^{-1}; Royer et al. 2006). Although their predicted oblateness is likely to be undetectable with the precision of our measurements, we should consider the angular diameter measured for these stars as the mean angular diameter. The rotational velocities of the F- and G-type stars observed are far below the critical, therefore they are assumed to be round.

3.1.2. Multiplicity

Our targets were selected to only include single stars because incoherent light from a companion affects the visibility of the primary star and biases the diameter measurement. We admit binary stars only with separations greater than 2 arcsec or

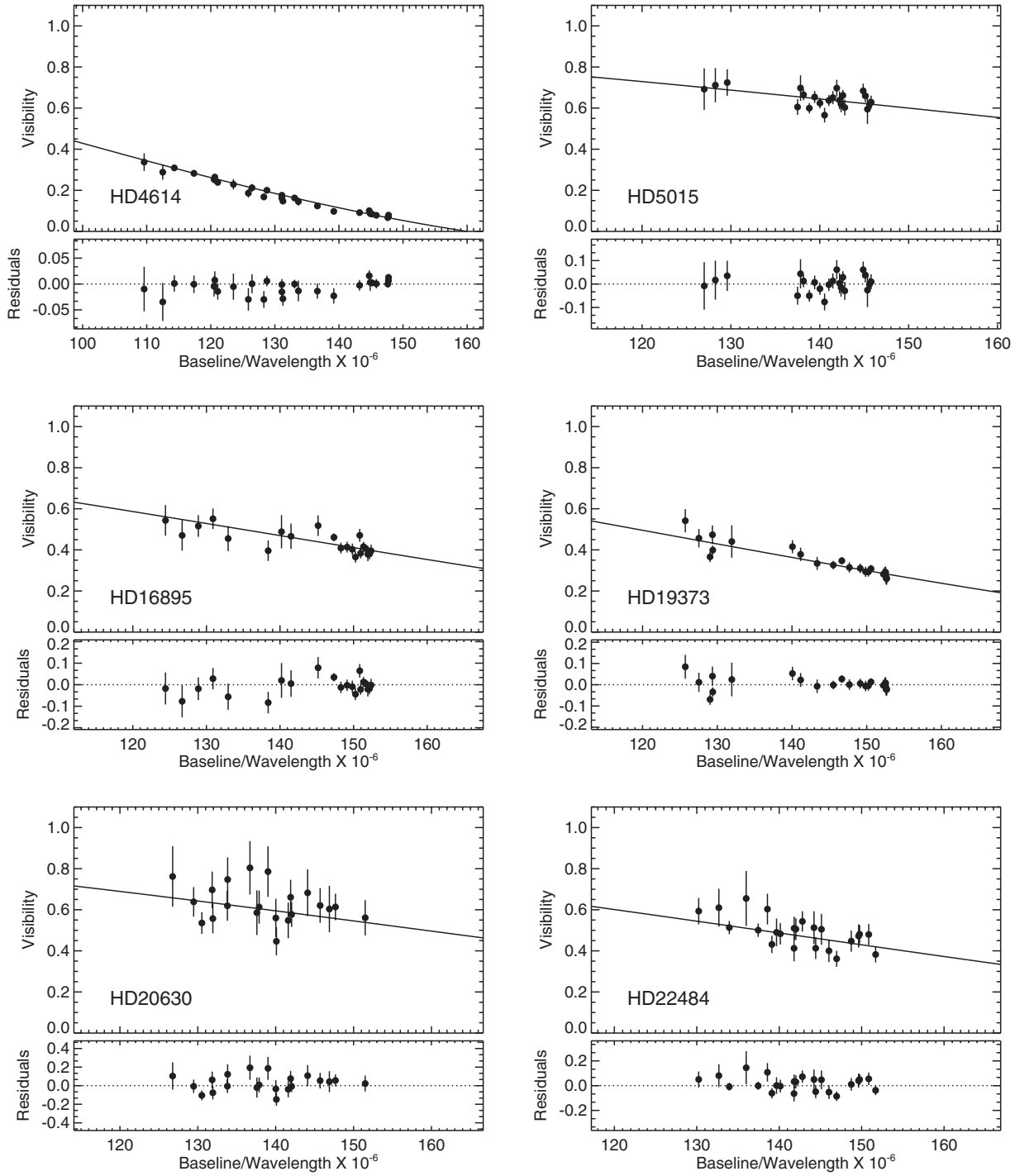

Figure 1. Calibrated observations plotted with the limb-darkened angular diameter fit for each star observed. See Section 3 and Table 5 for details.

with large ΔK magnitudes.[13] For example, the star HD 39587 (G0 V + M5 V; Han & Gatewood 2002) is a single-lined spectroscopic binary. Our data do not reveal the imprint of a companion (reduced $\chi^2 = 0.33$), and the diameter is assumed to be unaffected by the presence of a secondary star with the assumption that the Δ magnitude is quite large ($\Delta K > 4$ mag).

The diameter fit for the star HD 162003 has the largest reduced χ^2 of 2.23. Very recent radial velocity survey work has identified HD 162003 to have a long-term trend in radial velocity of $+220$ m s^{-1} yr^{-1} (Toyota et al. 2009).[14] We suspect that the reason our diameter fit for this star shows the highest value of reduced χ^2 is that we are actually detecting a mild signature of the secondary star in the visibilities. Another target in this survey HD 173667 is identified by Nidever et al. (2002) to have $\sigma_{\rm rms} = 124$ m s^{-1} over a period of 5165 days. However, unlike the diameter fit for HD 162003, the reduced χ^2 is typical of a fit from a single star (reduced $\chi^2 = 1.34$). Lastly, we note

[13] The formal limits to detection of companions with our instrument is currently unknown, but is thought to be sensitive to binaries with $\Delta K \lesssim 2.5$ (D. Raghavan 2009, private communication).

[14] Toyota et al. (2009) comment that the V_r trend is not attributed to the visual companion, HD 162004 $\sim 30''$ away.

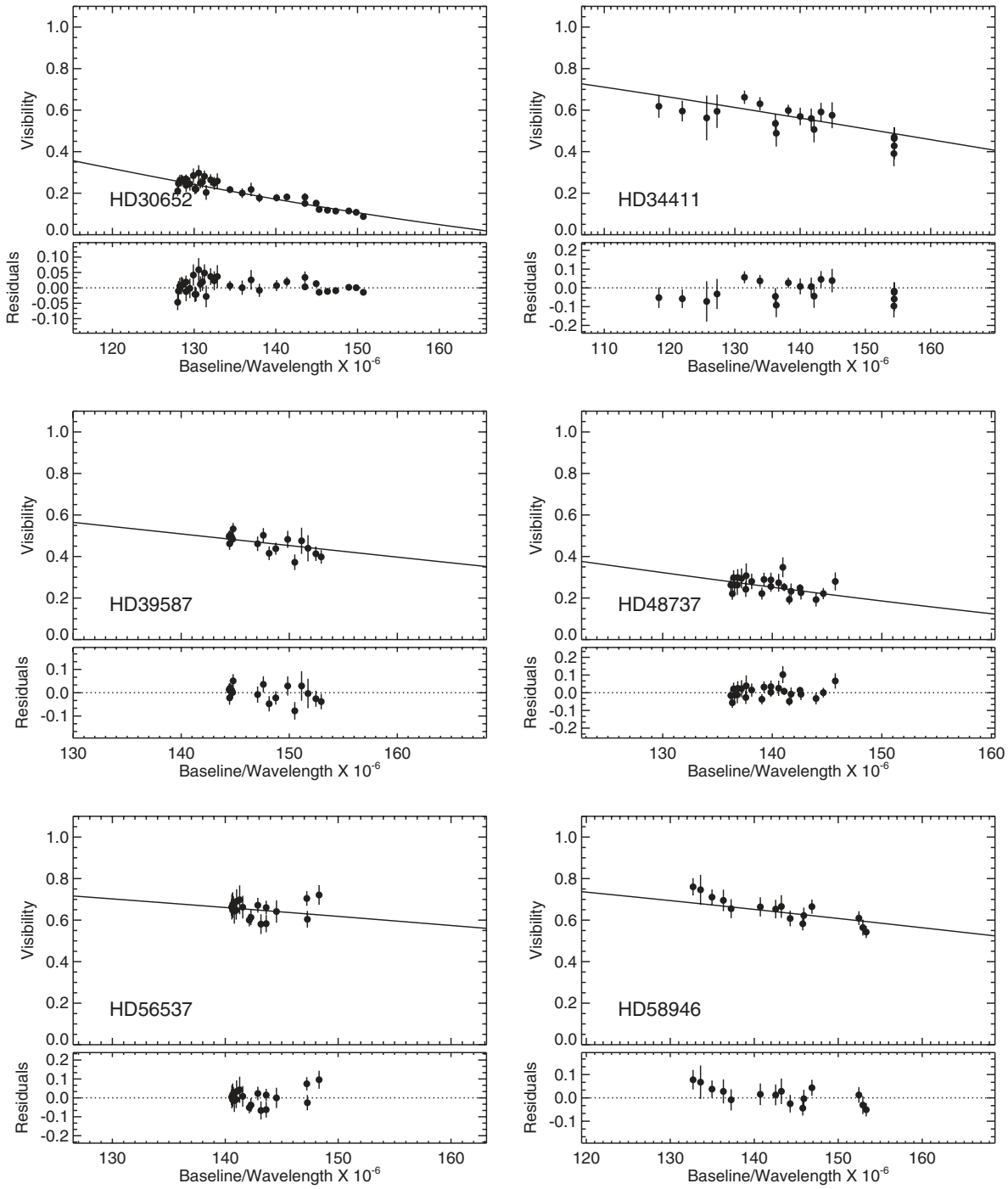

Figure 1. (Continued)

that the stars HD 4614 and HD 109358[15] were once referred to as spectroscopic binaries by Abt & Levy (1976). However, Morbey & Griffin (1987) disputed this result, and HD 109358 is now used as a radial velocity standard (for example, see Behr et al. 2009; Konacki 2005).

3.2. CHARA versus Palomar Testbed Interferometer Diameters

Angular diameters of a few dozen main-sequence stars measured with the Palomar Testbed Interferometer (PTI) were presented by van Belle & von Braun (2009). Their work provides measurements of 14 stars in common with the CHARA stars measured here and is the only alternate source of direct angular diameter measurements of our program stars. The longest baseline obtainable with PTI is 110 m, a factor of three shorter than those of the CHARA Array, and accurate measurements were quite difficult with this instrument due to the small angular sizes of these stars.

Table 6 lists the 14 stars in common with van Belle & von Braun (2009), the limb-darkened angular diameters and errors, and how many σ the two values differ from each other. For these stars, the errors on the PTI angular diameters are

[15] Which coincidentally has been assigned the name *Chara* (Hoffleit & Jaschek 1991).

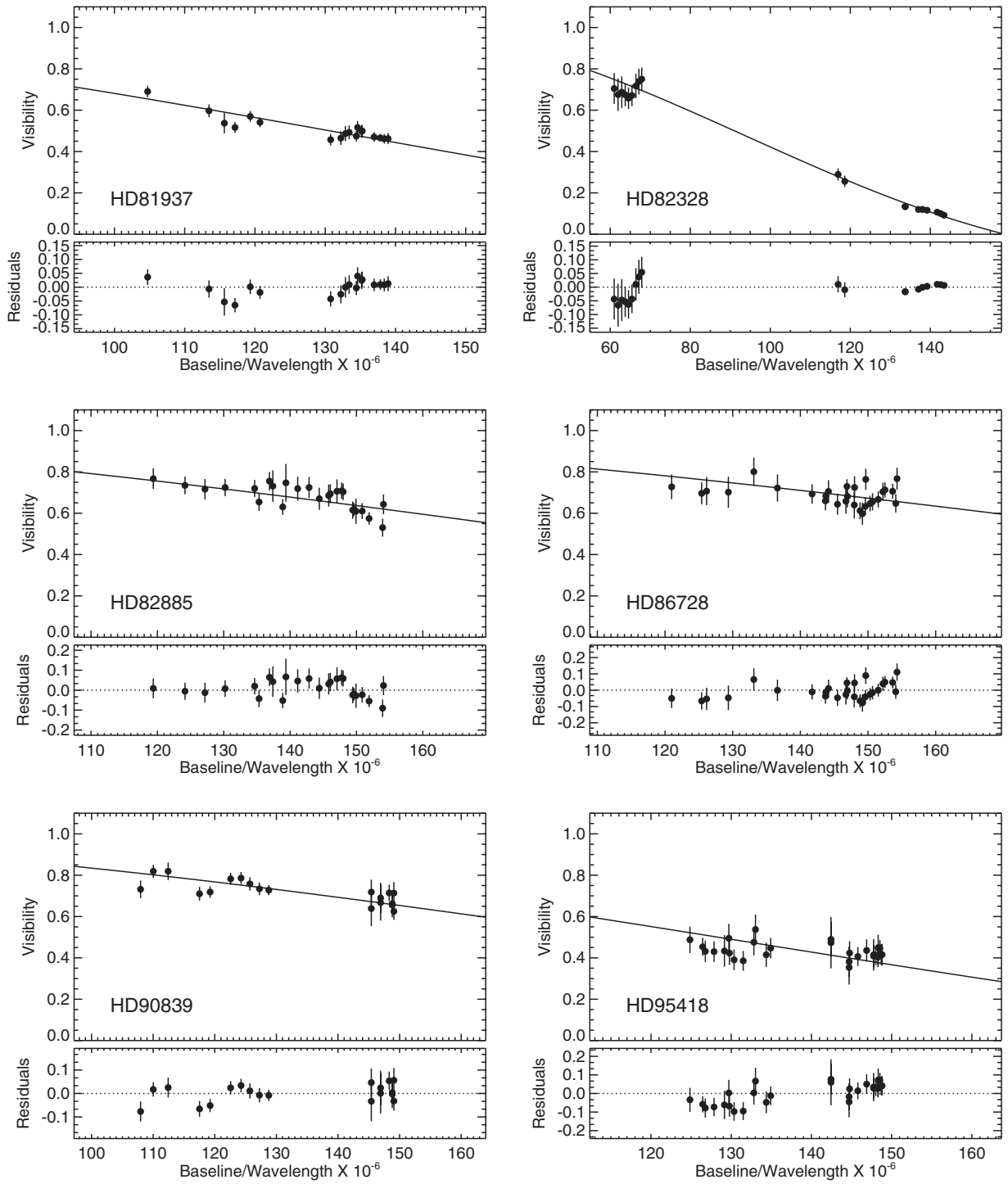

Figure 1. (Continued)

anywhere from 2 to 12 times (with an average of 6.5 times) the errors on the CHARA angular diameters. However, this comparison can still point to any systematic offsets in the results from each instrument. Comparing the angular diameters from this work and van Belle & von Braun (2009), we find that the weighted mean ratio of CHARA to PTI diameters is $\theta_{\rm CHARA}/\theta_{\rm PTI} = 1.052 \pm 0.062$. Van Belle & von Braun (2009) make this same comparison of their diameters compared to diameters from Baines et al. (2008), who used the CHARA Array to measure the diameters of exoplanet host stars, and find that the ratio of the four stars they have in common is $\theta_{\rm CHARA}/\theta_{\rm PTI} = 1.06 \pm 0.06$, very similar to the results found here, indicating again that there is a slight preference for smaller PTI diameters, and larger CHARA diameters, although the displacement is at the $<1\sigma$ level.

The preference to larger diameters compared to other interferometric measurements was also seen in Boyajian et al. (2009), where the diameters of the four Hyades giants were measured with the CHARA Array. In that work, two of the stars, ϵ Tau and δ^1 Tau, were measured previously with other interferometers (Mark III, NPOI, and PTI), all of which lead to smaller diameters than those measured with CHARA.

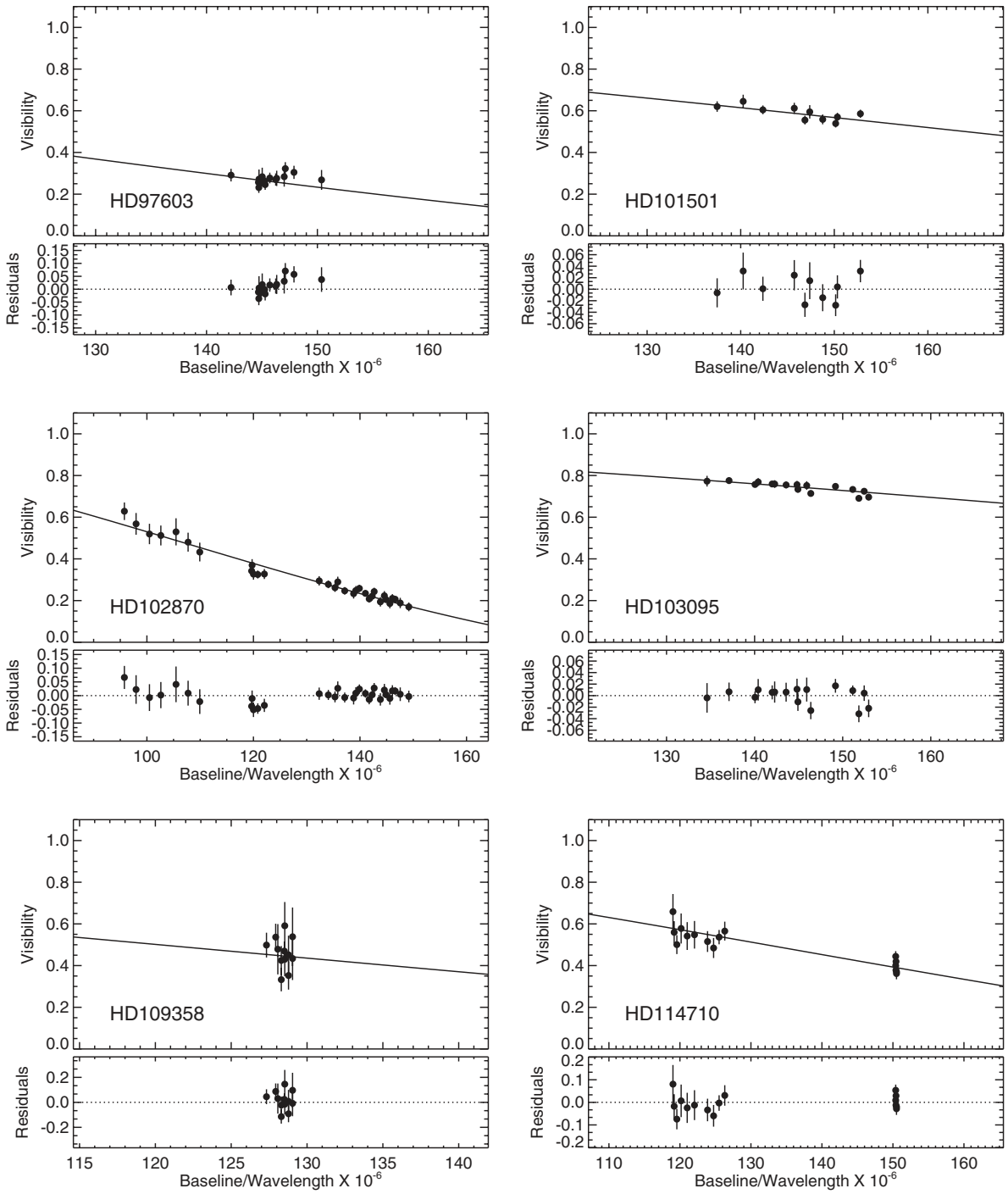

Figure 1. (Continued)

However, Boyajian et al. (2009) find that models for the Hyades age and metallicity match flawlessly with the CHARA observations, and the smaller angular diameters from other works in turn lead to temperatures that are too hot for these stars.

A main distinction that could lead to offsets in measured diameters is the estimated size of the calibrator stars. For instance, van Belle & von Braun (2009) discuss the calibrator selection in their work compared to Baines et al. (2008). Van Belle & von Braun (2009) set a limit to a sufficiently unresolved calibrator at CHARA to be <0.5 mas in diameter, a criterion which all but a few calibrators in this work meet. However, to investigate the possibility that the estimated size of the calibrators in this work is offset to the calibrators used in van Belle & von Braun (2009), we compare the estimated sizes of the calibrators in the Palomar Testbed Interferometer Calibrator Catalog (PTICC; van Belle et al. 2008) to the ones derived here. Twenty-nine of the 63 calibrators used in this work are included in the PTICC. Overall, the ratio of the estimated diameter of the calibrator in this work to the PTICC is 0.97 ± 0.06, a less than 1σ difference.

Twelve of the 14 stars in common with van Belle & von Braun (2009) were observed with calibrators whose diameters are also included in the PTICC. For each of these 12 calibrators,

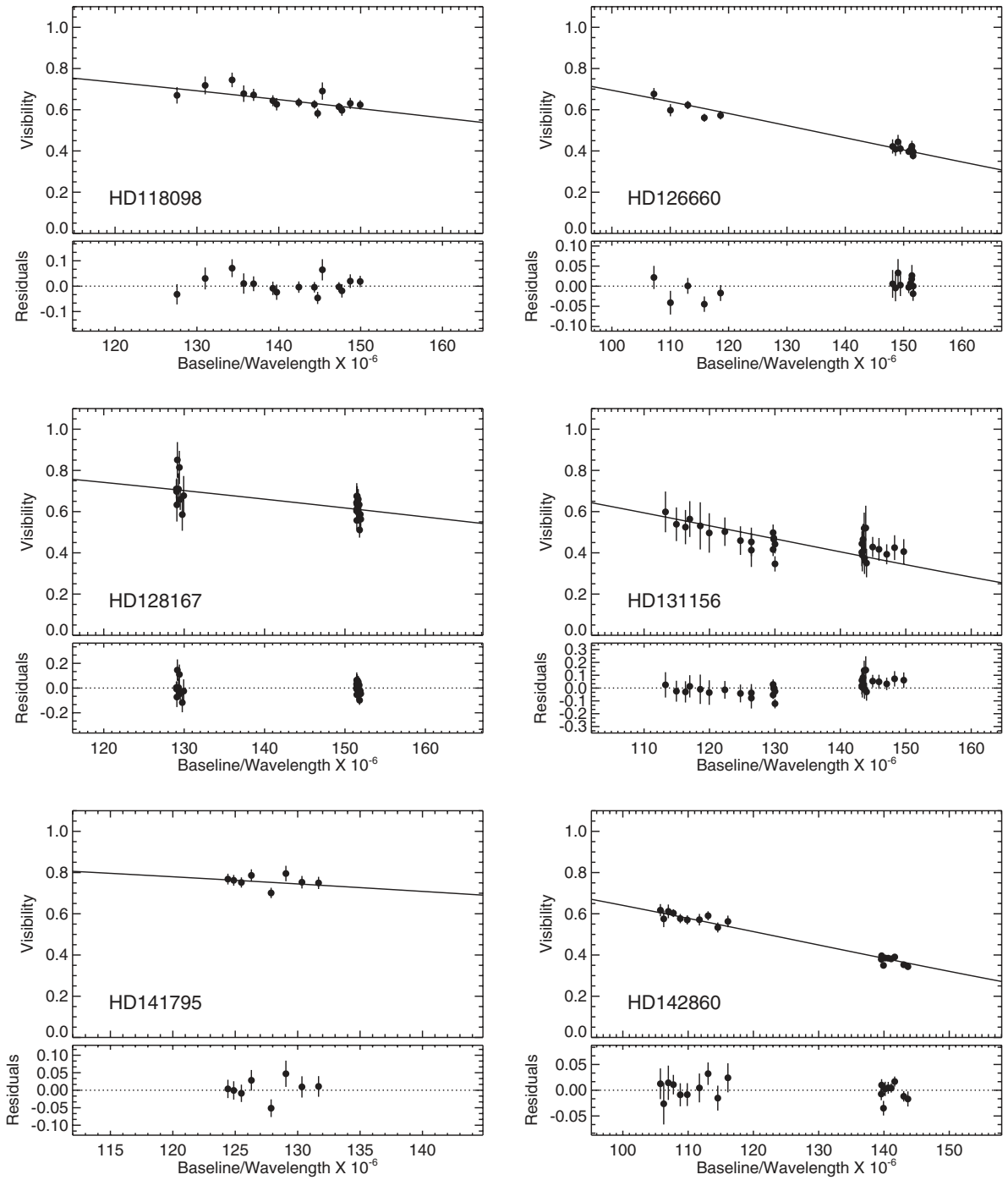

Figure 1. (Continued)

the estimated angular diameter $\theta_{\rm SED}$ is presented in Table 7, along with the ratio of the CHARA to PTI SED diameters. The object employing the calibrator is also listed in Table 7 along with the ratio of the CHARA to PTI measured limb-darkened diameters. Here, there is no pattern in the calibrator SED diameter ratio and the object diameter ratio. In fact, the effects of a slight offset in the calibrator's estimated diameter listed above (ratio $\theta_{\rm CHARA}/\theta_{\rm PTI} = 0.97 \pm 0.06$) would actually contribute counterproductively to the slight offset in the diameter measurements (ratio $\theta_{\rm CHARA}/\theta_{\rm PTI} = 1.05 \pm 0.06$). For instance, in the case of our data, the size of the calibrator $\theta_{\rm SED}$ is typically smaller, thus the true visibility of the calibrator would be greater (i.e., it would be more unresolved). If the true visibility of the calibrator is greater, it would in turn make the true visibility of the object larger in the calibration process. Thus, the object would appear more unresolved (having larger calibrated visibilities) if we were using a SED diameter of the same calibrator but with a larger value. Because we do not see the case of smaller CHARA diameters, this indicates that the calibrators are not the cause of any offset, if present, in each data set.

In Figure 2, we show a plot of the measured limb-darkened angular diameters presented here compared to the computed SED diameters for the stars in this survey. The 14 stars in common with the van Belle & von Braun (2009) work are highlighted in color, red indicating a CHARA measurement

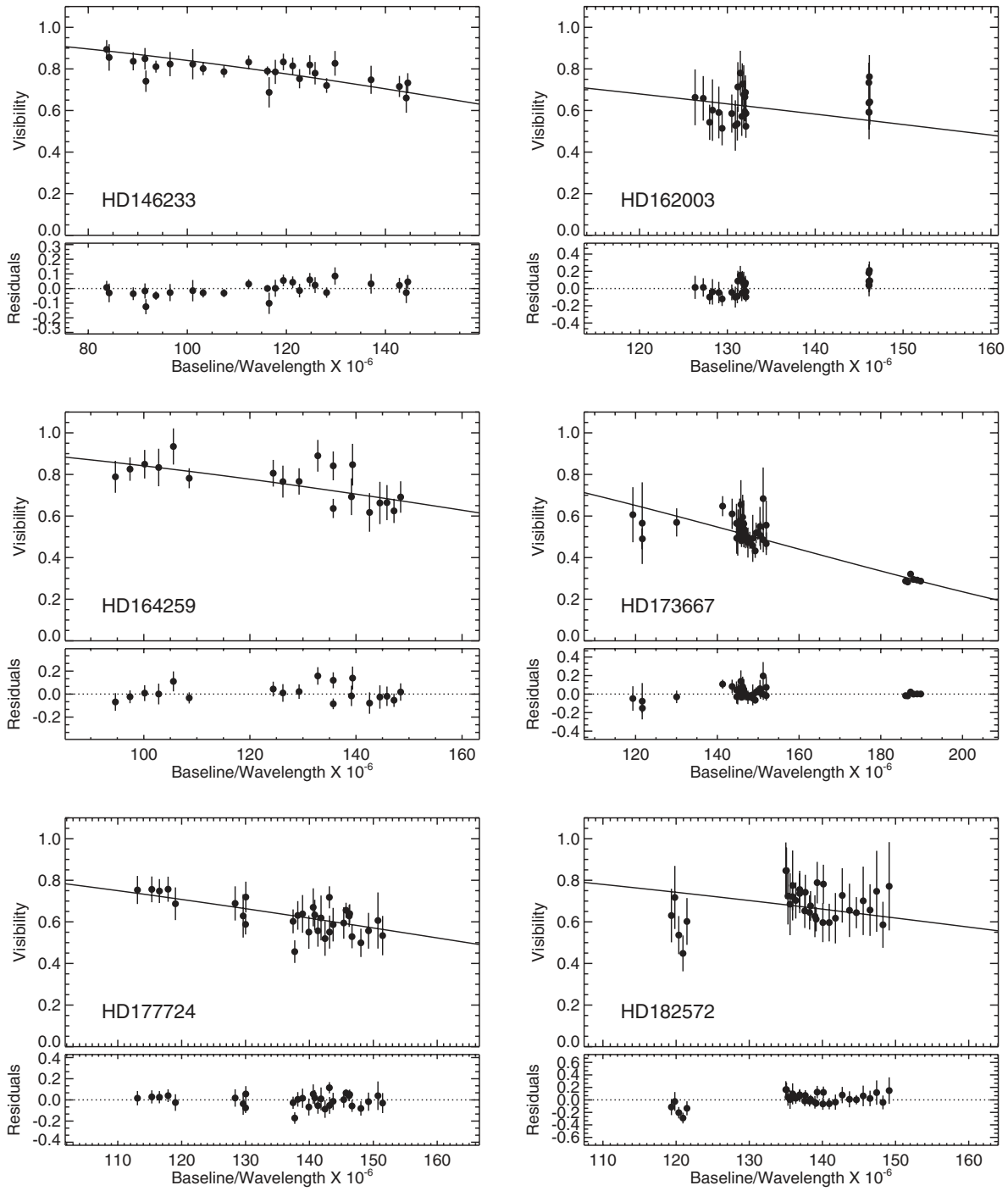

Figure 1. (Continued)

and blue for a PTI measurement. It is apparent here that the majority of the PTI diameters are deceptively low compared to the SED estimates.

Figure 3 shows the fractional difference of the measured limb-darkened versus SED angular diameter as a function of $(B-V)$ color index. For stars with a $(B-V) < 0.4$, the measured $\theta_{\rm LD}$ is always larger than the estimated $\theta_{\rm SED}$. There is a lot of scatter for stars redder than $(B-V)$ ~0.4, but no systematics are seen. However, in this region the two most metal-poor stars, HD 6582 and HD 103095, are the most extreme outliers, where $\theta_{\rm LD} > \theta_{\rm SED}$ in both cases. Additionally, HD 182572 ($B-V$ = 0.761; [Fe/H] = 0.33) is the most metal-rich star observed in this work and shows the largest disagreement here where $\theta_{\rm LD} < \theta_{\rm SED}$. Perhaps there is a lack of sufficient data to show if there is in fact a trend in either the color index or metallicity of a star and the estimated $\theta_{\rm SED}$.

4. STELLAR PARAMETERS

4.1. Bolometric Fluxes

We present new measures of the bolometric flux $F_{\rm BOL}$ for each star in this work that follows the method used previously in support of interferometric observations (van Belle et al. 2008;

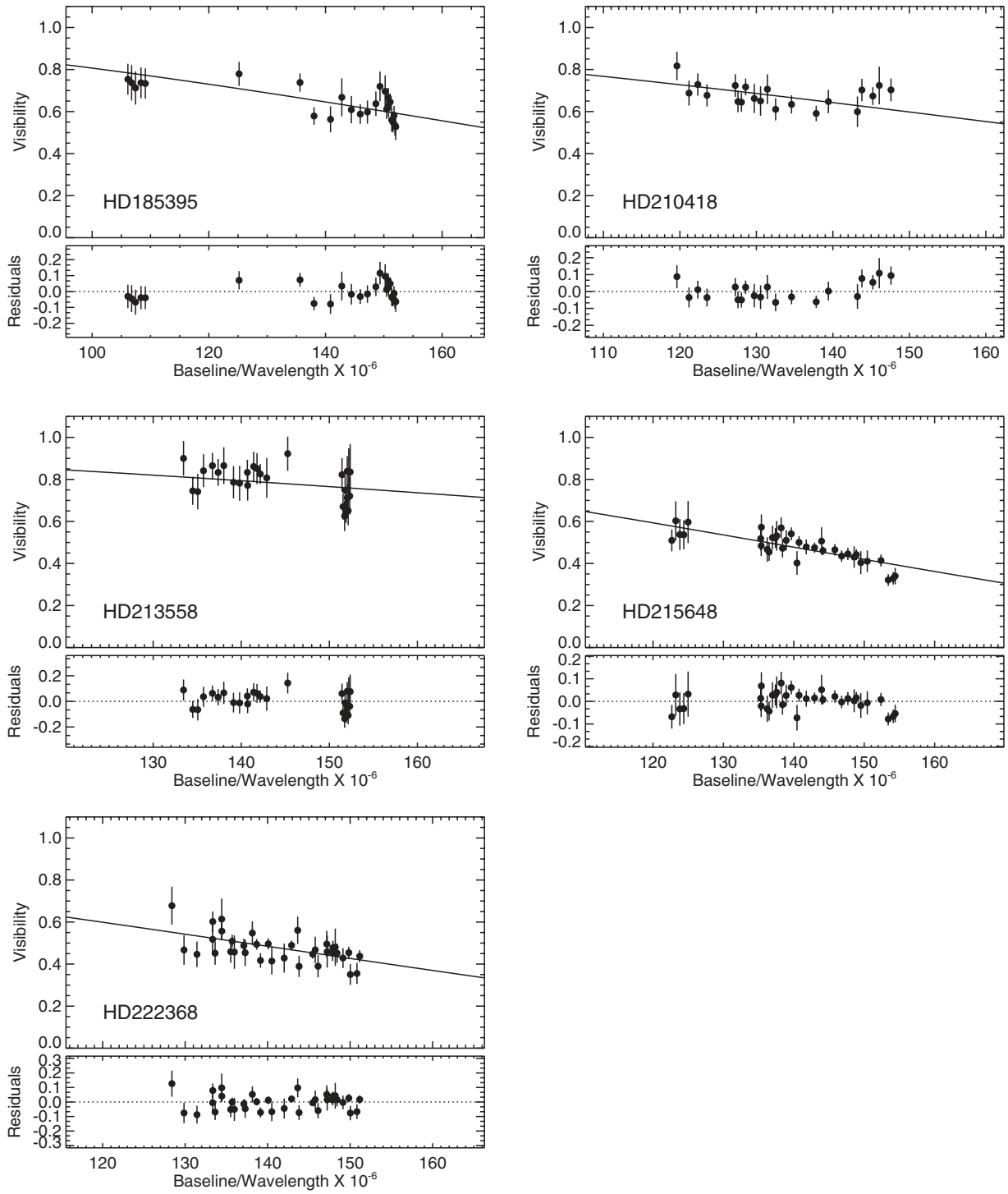

Figure 1. (Continued)

van Belle & von Braun 2009). The fit involves a collection of flux-calibrated photometry for each source available in the literature (see Table 8) that is subsequently fit with a template spectra from the Pickles (1998) library. Reddening is for the most part absent for the sample;[16] however, we fit it here to the photometric data using reddening corrections based upon the empirical reddening determination described by Cardelli et al. (1989), which differs little from van de Hulst's theoretical reddening curve number 15 (Johnson 1968; Dyck et al. 1996).

[16] Distance of the furthest star is ∼30 pc.

Uncertainties in $F_{\rm BOL}$ are for our data, on average 1.9%, and tend to be dominated by uncertainty in the reddening fit and poor photometry in the 0.6–1.2 μm range. Each science object is listed in Table 9 along with the fitting parameters: Pickles (1998) template spectral type, number of photometry points, and reduced χ^2 of the fit, as well as the resulting integrated $F_{\rm BOL}$ and A_V. In Figure 4, we show an example SED fit.

4.2. Luminosities, Temperatures, and Radii

These $F_{\rm BOL}$ measurements are then simply used in combination with the *Hipparcos* distance d to solve for the absolute

Table 6
CHARA versus PTI Angular Diameters

HD	CHARA $\theta_{LD} \pm \sigma$	Error (%)	PTI[a] $\theta_{LD} \pm \sigma$	Error (%)	$\Delta\theta_{LD}/\sigma_C$[b]
16895	1.103 ± 0.009	0.8	1.086 ± 0.056	5.2	0.3
19373	1.246 ± 0.008	0.6	1.331 ± 0.050	3.8	−1.7
20630	0.936 ± 0.025	2.7	0.895 ± 0.070	7.8	0.6
22484	1.081 ± 0.014	1.3	0.911 ± 0.123	13.5	1.4
30652	1.526 ± 0.004	0.3	1.409 ± 0.048	3.4	2.4
39587	1.051 ± 0.009	0.9	1.124 ± 0.056	5.0	−1.3
97603	1.328 ± 0.009	0.7	1.198 ± 0.053	4.4	2.4
109358	1.238 ± 0.030	2.4	1.138 ± 0.055	4.8	1.6
114710	1.127 ± 0.011	1.0	1.071 ± 0.057	5.3	1.0
126660	1.109 ± 0.007	0.6	1.130 ± 0.055	4.9	−0.4
142860	1.217 ± 0.005	0.4	1.161 ± 0.054	4.7	1.0
185144	1.254 ± 0.012	1.0	1.092 ± 0.057	5.2	2.8
215648	1.091 ± 0.008	0.7	1.022 ± 0.059	5.8	1.2
222368	1.082 ± 0.009	0.8	1.062 ± 0.057	5.4	0.3

Notes. Refer to Section 3.2 for details.
[a] From van Belle & von Braun (2009).
[b] Here, $\Delta\theta_{LD}$ is the difference between PTI and CHARA limb-darkened angular diameters, and σ_C is the combined error, $\sigma_C = (\sigma^2_{CHARA} + \sigma^2_{PTI})^{0.5}$.

luminosity L:

$$L = 4\pi d^2 F_{BOL}. \quad (3)$$

Additionally, we can express the effective temperature of a star as defined through the Stephan–Boltzmann law:

$$F = \sigma T^4_{EFF}, \quad (4)$$

where F is the total emergent flux of the star and σ is the Stefan–Boltzmann constant. Transforming this equation to observables at Earth, we arrive at the expression

$$F_{BOL} = \frac{1}{4}\theta^2 \sigma T^4_{EFF}. \quad (5)$$

The effective temperature T_{EFF} is found by solving Equation (5) in terms of F_{BOL} and θ_{LD}, where in Equation (6), F_{BOL} is in units of 10^{-8} erg s^{-1} cm^{-2} and θ_{LD} is in units of mas. This yields the relation

$$T_{EFF} = 2341(F_{BOL}/\theta^2)^{0.25}. \quad (6)$$

Finally, using *Hipparcos* parallaxes from van Leeuwen (2007), we transform the measured angular diameters of these stars into linear radii R. Each of these derived parameters are presented in Table 10. Graphical representations of these data sets are presented in Figures 5 and 6.

5. DISCUSSION

5.1. Empirical Temperature Relations

With the results in Table 10, we may begin to define a foundation of empirically based color–temperature relations. These relationships are extremely useful in extending our knowledge to a larger number of stars, at distances too far to accurately resolve their sizes. For giants and supergiants, temperature scales accurate to the 2.5% level are obtainable, and are currently limited by the distances to these objects, not the sensitivities of our interferometric observations (van Belle et al. 1999, 2009). Recently, and more similarly comparable to this work, van Belle & von Braun (2009) present relations for main-sequence stars, ranging from $(V-K) \sim 0.0$ to 4.0 (spectral types of ∼A-M). These scales are slightly better than the aforementioned evolved classes of stars and are accurate to the ∼2% level. The authors note here that the limitations to these relations are in the angular diameter measurements themselves.

5.1.1. $(B-V)$–T_{EFF}

Here, we derive color–temperature relations based on the precise T_{EFF} measurements presented in Table 10 in the form of a sixth-order polynomial. The solution for the $(B-V)$

Table 7
CHARA versus PTI Calibrators

Calibrator HD	CHARA θ_{SED} (mas)	PTI[a] θ_{SED} (mas)	Calibrator SED $\theta_{CHARA}/\theta_{PTI}$	Object HD	Object Measured $\theta_{CHARA}/\theta_{PTI}$[b]
20675	0.415 ± 0.012	0.424 ± 0.020	0.98 ± 0.05	16895	1.02 ± 0.05
20675	0.415 ± 0.012	0.424 ± 0.020	0.98 ± 0.05	19373	0.94 ± 0.04
22879	0.342 ± 0.021	0.369 ± 0.009	0.93 ± 0.06	20630	1.05 ± 0.09
22879	0.342 ± 0.021	0.369 ± 0.009	0.93 ± 0.06	22484	1.19 ± 0.16
28355	0.425 ± 0.030	0.401 ± 0.012	1.06 ± 0.08	30652	1.08 ± 0.04
30739	0.461 ± 0.018	0.544 ± 0.025	0.85 ± 0.05	30652	1.08 ± 0.04
31295	0.439 ± 0.043	0.470 ± 0.022	0.93 ± 0.10	30652	1.08 ± 0.04
38558	0.422 ± 0.008	0.442 ± 0.033	0.95 ± 0.07	39587	0.94 ± 0.05
43042	0.591 ± 0.030	0.655 ± 0.017	0.90 ± 0.05	39587	0.94 ± 0.05
99285	0.456 ± 0.017	0.454 ± 0.026	1.00 ± 0.07	97603	1.11 ± 0.05
110897	0.492 ± 0.022	0.504 ± 0.009	0.98 ± 0.05	109358	1.09 ± 0.06
132254	0.520 ± 0.015	0.542 ± 0.013	0.96 ± 0.04	126660	0.98 ± 0.05
193664	0.494 ± 0.019	0.552 ± 0.011	0.89 ± 0.04	185144	1.15 ± 0.06
211976	0.373 ± 0.013	0.377 ± 0.009	0.99 ± 0.04	215648	1.07 ± 0.06
214923	0.611 ± 0.029	0.552 ± 0.094	1.11 ± 0.20	215648	1.07 ± 0.06
216735	0.321 ± 0.022	0.330 ± 0.020	0.97 ± 0.09	215648	1.07 ± 0.06
216735	0.321 ± 0.022	0.330 ± 0.020	0.97 ± 0.09	222368	1.02 ± 0.06
222603	0.577 ± 0.032	0.533 ± 0.014	1.08 ± 0.07	222368	1.02 ± 0.06

Notes. Refer to Section 3.2 for details.
[a] From the PTICC (van Belle et al. 2008).
[b] The limb-darkened diameter presented here versus the value in van Belle & von Braun (2009).

Table 8
Target Photometry

Object HD	System/ Wavelength	Bandpass Bandwidth	Value (mag)	Error (mag)	Reference
HD 4614	1240	248	2.41	0.05	Selby et al. (1988)
HD 4614	1250	250	2.36	0.05	Johnson (1965b)
HD 4614	1250	250	2.36	0.05	Johnson et al. (1966)
HD 4614	1250	250	2.35	0.05	Johnson et al. (1968)
HD 4614	1250	250	2.35	0.05	Voelcker (1975)
HD 4614	1250	250	2.41	0.05	Blackwell et al. (1990)
HD 4614	1270	254	2.35	0.05	Bergeat & Lunel (1980)
HD 4614	1620	324	2.02	0.05	Bergeat & Lunel (1980)
HD 4614	1650	330	2.02	0.05	Johnson et al. (1968)
HD 4614	1650	330	2.02	0.05	Voelcker (1975)

Notes. Refer to Section 2.3 for details.

(This table is available in its entirety in a machine-readable form in the online journal. A portion is shown here for guidance regarding its form and content.)

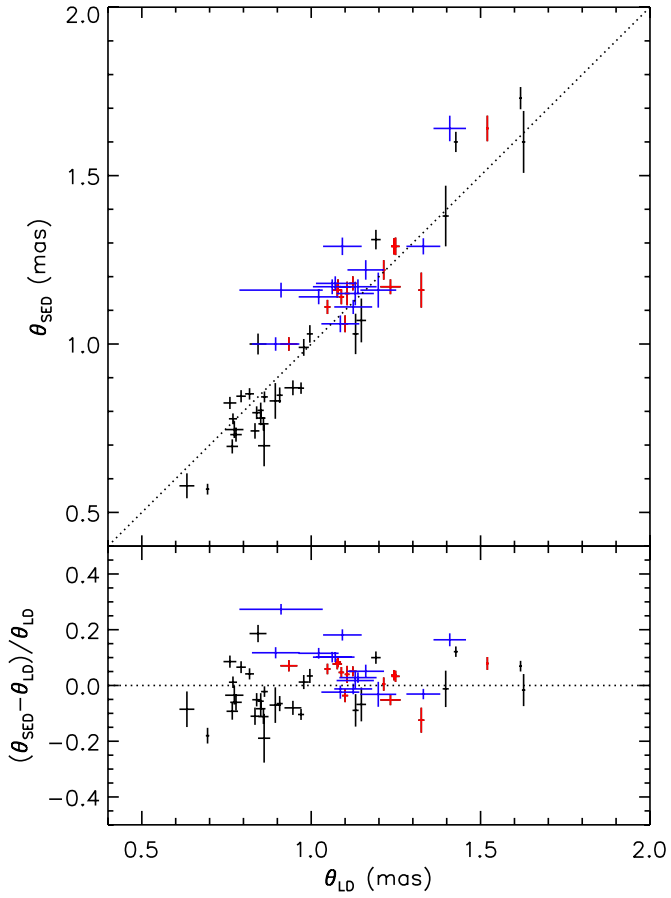

Figure 2. Top: plot showing the measured limb-darkened angular diameters vs. the SED angular diameters and the 1σ errors (black). Measurements for the 14 stars in common with this work are highlighted in color with red indicating a CHARA measurement presented in this paper and blue for a PTI measurement measured in van Belle & von Braun (2009). Bottom: plot showing the fractional difference between the SED and limb-darkened angular diameters. The dotted line shows an equal agreement of both measurements. See Section 3.2 and Tables 5 and 6 for details.

(A color version of this figure is available in the online journal.)

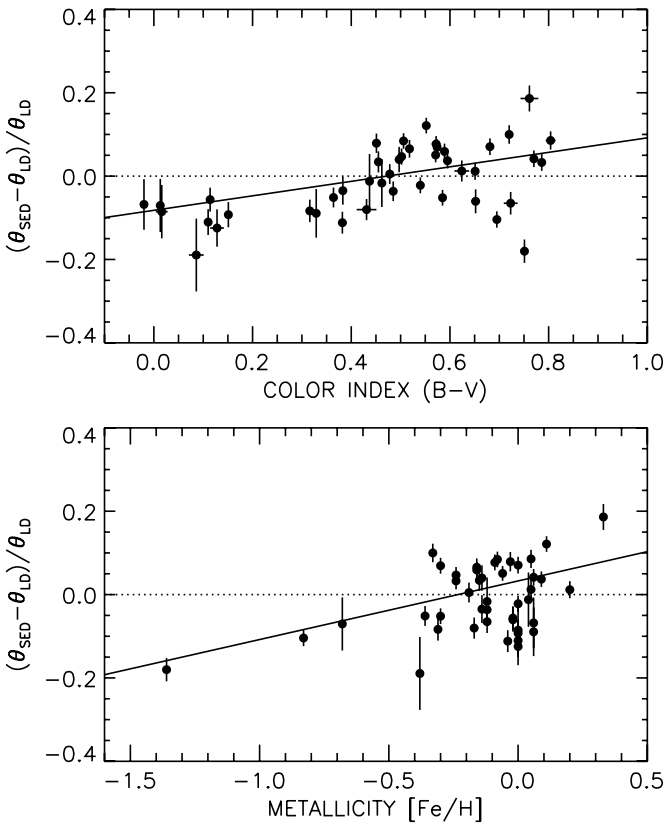

Figure 3. Top: the difference between limb-darkened angular diameters and the SED angular diameters from this work vs. $(B-V)$ color index. Bottom: the same as above with respect to metallicity. The dotted line shows an equal agreement of both measurements. A provisional fit to the data is shown as a solid line and is suspect to a cautious interpretation due to the sparse amount of data available. See Section 3 for details.

color–temperature relation is expressed as

$$\log T_{\rm EFF} = 3.9680 \pm 0.0025 - 0.2633 \pm 0.0876(B-V) - 3.2195 \pm 1.3407(B-V)^2 + 15.3548 \pm 6.8551(B-V)^3 - 27.2901 \pm 15.7373(B-V)^4 + 19.9193 \pm 16.8465(B-V)^5 - 4.5127 \pm 6.8539(B-V)^6 \quad \text{for } 0.05 < (B-V) < 0.80 \text{ and } [\text{Fe/H}] > -0.75. \tag{7}$$

This solution, in the form of a sixth-order polynomial, defines the shape of the data inflection point at $(B-V) \sim 0.3$ better than a lower order polynomial function, as well as a power-law

Table 9
Bolometric Fluxes

Star HD	Template Sp.Ty.	No. of PHOT	Reduced χ^2	$F_{BOL} \pm \sigma$ (10^{-8} erg s^{-1} cm^{-2})	$A_V \pm \sigma$ (mag)
4614	G0V	80	1.04	113.90 ± 1.71	0.001 ± 0.014
5015	F8V	95	0.74	31.50 ± 0.56	0.005 ± 0.016
6582	G5V	165	2.63	24.48 ± 0.39	0.000 ± 0.014
10780	K0V	86	0.75	16.43 ± 0.33	0.000 ± 0.018
16895	F6V	94	0.70	58.21 ± 1.04	0.000 ± 0.016
19373	G0V	89	0.41	63.29 ± 0.93	0.016 ± 0.013
20630	G5V	205	0.59	32.46 ± 0.55	0.000 ± 0.015
22484	G0V	171	0.33	51.23 ± 0.69	0.000 ± 0.012
30652	F6V	251	0.72	139.80 ± 1.50	0.000 ± 0.009
34411	G1V	151	0.49	35.01 ± 0.45	0.000 ± 0.011
39587	G0V	139	0.28	46.44 ± 0.78	0.011 ± 0.015
48737	F5III	85	0.60	115.20 ± 2.37	0.000 ± 0.018
56537	A5V	136	1.11	95.40 ± 2.18	0.000 ± 0.019
58946	F0V	156	0.41	54.87 ± 0.88	0.020 ± 0.014
81937	F02IV	69	1.69	85.77 ± 1.88	0.035 ± 0.019
82328	F6.5IV	96	0.32	139.70 ± 2.81	0.000 ± 0.018
82885	G8V	189	1.32	19.57 ± 0.18	0.032 ± 0.008
86728	G5V	150	0.26	19.63 ± 0.39	0.000 ± 0.017
90839	F8V	83	0.43	31.69 ± 0.82	0.000 ± 0.023
95418	A0IV	106	0.82	339.90 ± 7.05	0.038 ± 0.017
97603	A4V	105	1.55	250.90 ± 3.87	0.053 ± 0.013
101501	G6.5V	138	0.41	21.27 ± 0.30	0.011 ± 0.012
102870	G0V	222	0.35	96.43 ± 1.41	0.000 ± 0.013
103095	G9V	244	3.85	8.27 ± 0.08	0.000 ± 0.009
109358	G0V	137	0.57	52.11 ± 0.84	0.000 ± 0.014
114710	G0V	216	0.43	52.49 ± 0.56	0.000 ± 0.010
118098	A5V	104	2.29	111.80 ± 1.57	0.000 ± 0.013
126660	F7V	98	0.50	63.08 ± 1.47	0.000 ± 0.020
128167	F2V	182	1.88	44.52 ± 0.54	0.062 ± 0.010
131156	G8V	90	1.45	46.18 ± 1.05	0.043 ± 0.019
141795	A5V	101	1.13	83.87 ± 2.05	0.020 ± 0.020
142860	F6V	156	0.31	77.38 ± 1.30	0.014 ± 0.014
146233	G3.5V	116	0.62	17.65 ± 0.46	0.000 ± 0.022
162003	F6V	96	0.44	39.22 ± 0.95	0.000 ± 0.021
164259	F3.5V	134	0.43	36.34 ± 0.74	0.000 ± 0.018
173667	F6V	84	0.33	55.02 ± 1.19	0.002 ± 0.019
177724	A0V	163	1.16	191.50 ± 3.12	0.002 ± 0.014
182572	G8IV	95	1.86	26.66 ± 0.63	0.000 ± 0.021
185144	K0V	240	0.72	39.93 ± 0.56	0.000 ± 0.012
185395	F2V	143	0.25	40.91 ± 0.86	0.015 ± 0.018
210418	A2IV	83	1.21	98.86 ± 2.46	0.000 ± 0.022
213558	A0V	109	0.94	93.04 ± 2.21	0.015 ± 0.020
215648	F8V	154	0.66	57.33 ± 1.05	0.000 ± 0.016
222368	F8V	279	0.40	60.95 ± 0.99	0.000 ± 0.014

Notes. For details, see Section 4.1.

function (see Figure 7). We are also cautious that the stars with low metallicity will affect the $(B-V)$–T_{EFF} transformation too severely to be useful for stars of solar-type abundances, and we refrain from using these in this analysis.[17] A preliminary fit to the data yields a median deviation in temperature of 68 K, and a median deviation in temperature of 55 K is found for an identical solution if we omit three obvious outliers lying more than 5σ away, HD 210418, HD 182572, and HD 162003 (offset of -6.7σ, -5.7σ, and $+6.5\sigma$, respectively). The statistical summary for the solution to the polynomial can be found in Table 11.[18]

In Figure 7, we show our data and the solution for the fit. We also show the solution from several other sources, Code et al. (1976), Gray (1992), and Lejeune et al. (1998). All the solutions shown here are approximately identical in the range of $(B-V) > 0.45$.

Similar to our work, the results from Code et al. (1976) are derived solely on empirical measurements. In that milestone paper, Code et al. (1976) measure the diameters of 32 stars using the NSII, all being objects hotter than the Sun and most having evolved luminosity classes. We show in Figure 7 the nine data points from Code et al. (1976) that have a $(B-V) > 0$ (∼A-type and later) with luminosity class V or IV (eight A-type objects and one F-type object), as well as

[17] There are two stars, HD 6582 and HD 103095, with metallicity [Fe/H] < -0.75.

[18] A fit to our data with a power relation yields an initial solution with a median deviation in temperature of 125 K, and 101 K removing the points with low metallicity. A deviation of 92 K is found after removing outliers lying more than 3σ from the fit, almost double the value we find for the polynomial fit.

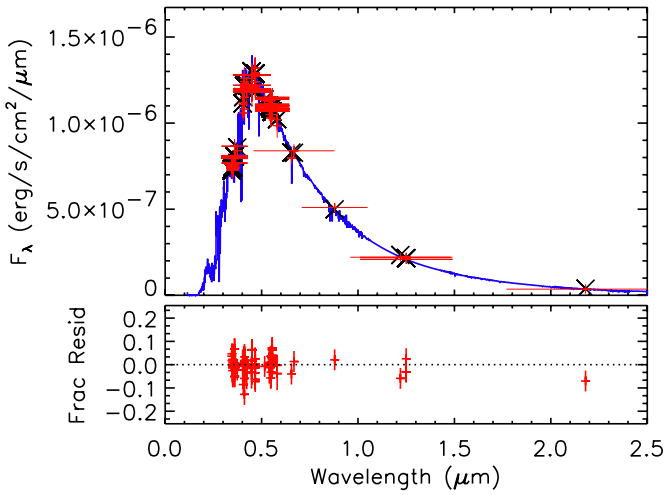

Figure 4. Example of SED fit for HD 142860. The (red) pluses indicate flux-calibrated photometry from the literature with corresponding errors (y-direction) and bandwidth of the filter (x-direction). The (black) crosses show the flux value of the spectral template integrated over the filter transmission for each point. The spectral template is plotted by a blue line. The lower panel shows the residuals. See Section 4 for details.

(A color version of this figure is available in the online journal.)

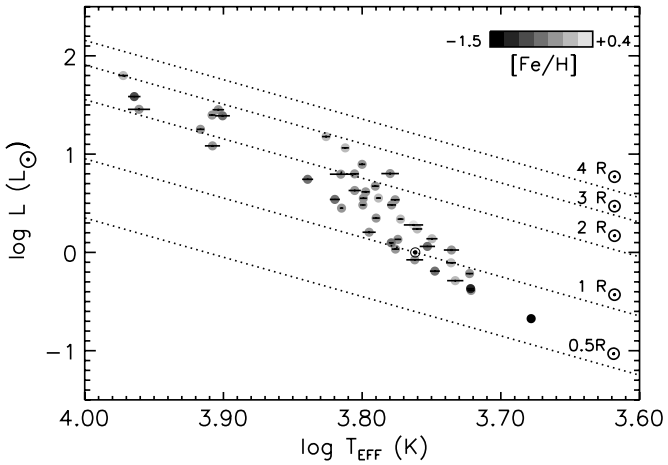

Figure 5. Luminosities and temperatures of the stars in the survey are plotted with their 1σ errors. Lines of constant radii are plotted as dotted lines. The shading of the symbol represents the metallicity of the star [Fe/H]. See Section 4.2 for details.

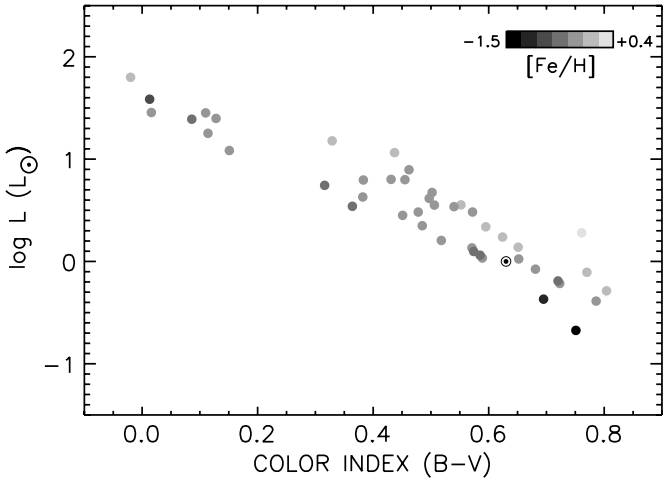

Figure 6. Luminosity and $(B-V)$ color index plotted of the stars in this survey. The shading of the symbol represents the metallicity of the star [Fe/H]. See Section 4.2 for details.

Table 10
Radii, Luminosities, and Temperatures

Star HD	R ($R_\odot$)	L ($L_\odot$)	$T_{\rm EFF}$ (K)
4614	1.039 ± 0.004	1.252 ± 0.019	6003 ± 24
5015	1.743 ± 0.023	3.432 ± 0.061	5963 ± 44
6582	0.790 ± 0.009	0.428 ± 0.007	5264 ± 32
10780	0.825 ± 0.021	0.516 ± 0.010	5396 ± 72
16895	1.319 ± 0.011	2.235 ± 0.040	6157 ± 37
19373	1.412 ± 0.009	2.181 ± 0.032	5915 ± 29
20630	0.919 ± 0.025	0.841 ± 0.014	5776 ± 81
22484	1.622 ± 0.024	3.042 ± 0.042	5997 ± 44
30652	1.323 ± 0.004	2.822 ± 0.030	6516 ± 19
34411	1.331 ± 0.021	1.732 ± 0.022	5749 ± 48
39587	0.979 ± 0.009	1.081 ± 0.018	5961 ± 36
48737	2.710 ± 0.021	11.574 ± 0.238	6480 ± 39
56537	2.777 ± 0.047	28.306 ± 0.648	8007 ± 77
58946	1.655 ± 0.028	5.542 ± 0.089	6899 ± 63
81937	2.902 ± 0.026	15.086 ± 0.330	6693 ± 45
82328	2.365 ± 0.008	7.871 ± 0.158	6300 ± 33
82885	1.003 ± 0.016	0.784 ± 0.007	5434 ± 45
86728	1.247 ± 0.021	1.378 ± 0.027	5612 ± 52
90839	1.091 ± 0.020	1.605 ± 0.042	6233 ± 68
95418	3.021 ± 0.038	63.015 ± 1.307	9377 ± 75
97603	2.557 ± 0.020	24.973 ± 0.385	8085 ± 42
101501	0.940 ± 0.010	0.609 ± 0.009	5270 ± 32
102870	1.681 ± 0.008	3.572 ± 0.052	6132 ± 26
103095	0.681 ± 0.006	0.212 ± 0.002	4759 ± 20
109358	1.123 ± 0.028	1.151 ± 0.018	5653 ± 72
114710	1.106 ± 0.011	1.357 ± 0.014	5936 ± 33
118098	2.079 ± 0.025	17.885 ± 0.252	8247 ± 52
126660	1.733 ± 0.011	4.131 ± 0.096	6265 ± 41
128167	1.431 ± 0.023	3.461 ± 0.042	6594 ± 55
131156	0.863 ± 0.011	0.645 ± 0.015	5580 ± 46
141795	1.783 ± 0.040	12.134 ± 0.296	8084 ± 102
142860	1.472 ± 0.007	3.039 ± 0.051	6294 ± 29
146233	1.166 ± 0.026	1.058 ± 0.028	5433 ± 69
162003	2.329 ± 0.067	6.343 ± 0.153	6014 ± 90
164259	1.961 ± 0.071	6.251 ± 0.127	6529 ± 118
173667	2.064 ± 0.017	6.296 ± 0.136	6376 ± 39
177724	2.449 ± 0.046	38.492 ± 0.627	9205 ± 95
182572	1.379 ± 0.042	1.904 ± 0.045	5787 ± 92
185144	0.776 ± 0.008	0.410 ± 0.006	5255 ± 31
185395	1.697 ± 0.030	4.265 ± 0.090	6381 ± 65
210418	2.623 ± 0.083	24.549 ± 0.610	7951 ± 97
213558	2.143 ± 0.074	28.552 ± 0.678	9131 ± 167
215648	1.912 ± 0.016	4.722 ± 0.087	6167 ± 36
222368	1.595 ± 0.014	3.555 ± 0.058	6288 ± 37

Notes. For details, see Section 4.2.

Table 11
Solutions to $T_{\rm EFF}$ Relations

	$(B-V)$	$(V-K)$	Spectral Type
Equation in text	(8)	(9)	(10)
n ...	39	44	41
Range ...	0.05–0.80[a]	0.0–2.0	A0–K0[a]
Reduced χ^2 ...	5.97	6.04	12.1
Median $dT_{\rm EFF}$ ...	55	64	90

Notes. Refer to Section 5.1 for details.
[a] Metallicity [Fe/H] > −0.75.

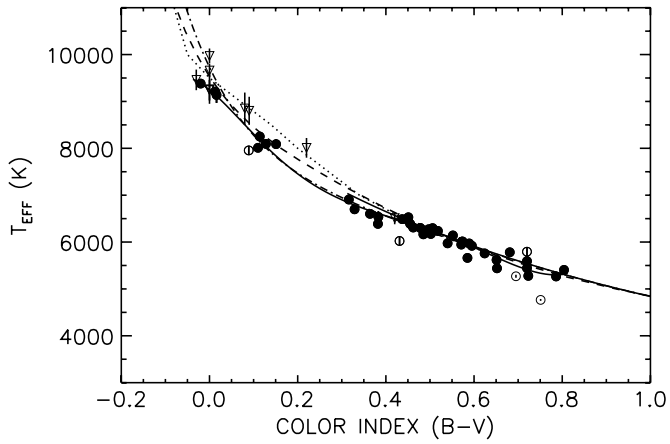

Figure 7. Data and solution for the temperature–$(B-V)$ relation shown as circles and a solid line, respectively. The data omitted from the fit are plotted as open circles and can be identified (from left to right) as HD 210418, HD 162003, HD 6582, HD 182572, and HD 103095. The inverted triangles show the data from Code et al. (1976) and the empirical solution based on these data is plotted as a dotted line. The 1σ errors in temperature are displayed, but are typically smaller than the data point. The dash-dotted line is the calibration presented in Gray (1992), using a menagerie of data sources (see reference). The solution for solar metallicity from Casagrande et al. (2010) is shown as a triple-dot-dashed line. The entirely model-based solution from Lejeune et al. (1998; dashed line) is also shown. For details, see Section 5.1.1 and Equation (8).

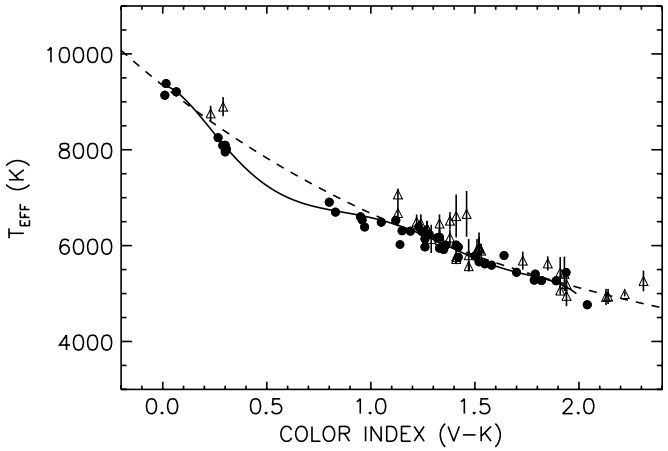

Figure 8. Data points plotted as filled circles depict the observations presented here, and open triangles are the measurements from van Belle & von Braun (2009). The 1σ errors in temperature are shown, but are typically smaller than the data point. Our solution for the temperature–$(V-K)$ relation shown as a solid line (Equation (9)), whereas the relation from van Belle & von Braun (2009) is shown as a dashed line. For details, see Section 5.1.2 and Equation (9).

the fit from Code et al. (1976). Comparing this fit to ours, we note that it is a few hundred Kelvin hotter than our own for $0.05 < (B-V) < 0.3$, converging at the bluest range of $(B-V) \sim 0$, as well as the reddest range $(B-V) \sim 0.4$. The offset is likely strongly connected to the fit's dependence on the sparse amount of data in this intermediate range.

The function presented in Gray (1992) also uses a sixth-order polynomial to fit $(B-V)$ to $T_{\rm EFF}$ (their Equation (15.14)). This is a fit to a compilation of data, including the NSII data from Code et al. (1976), but mostly data obtained via the infrared flux method (IRFM; see Blackwell & Shallis 1977), yielding a semi-empirical approach in obtaining the angular diameter, and consequentially the effective temperature, of a star. There is an impressive correlation with our fit throughout the range of $(B-V)$ colors. A deviation only begins to appear at the bluest colors ($(B-V) \sim 0$). Our sample stops here, but it can be readily seen in Gray (1992) that there is another inflection point at this color index, producing a steeper curve at more negative color indices. Because of this, we caution against the use of the relation presented here for colors bluer than $(B-V) < 0.05$.

As an update, the work presented in Casagrande et al. (2010) presents an excellent analysis and improvement to the IRFM temperature scales that have been proposed over the years. In Figure 7, we also show the Casagrande et al. (2010) solution for solar metallicity for comparison (valid in the ranges of $(B-V) > 0.3$). This relation is distinguishable from ours only when $0.3 < (B-V) < 0.4$, where at this point, the Casagrande et al. (2010) relation begins to predict ~100 K higher temperatures. However, we suspect that the likely explanation for this difference is that their solution is in the form of a third-order polynomial, which has been shown not to model the inflection point in this region properly.

For an additional comparison on the $(B-V)$ to $T_{\rm EFF}$ relations, we also show the entirely model-based solution from Lejeune et al. (1998; dashed line). This solution is intermediate to ours (as well as the one in Gray 1992) and the one from Code et al. (1976) for the mid-A- to mid-F-type stars.

The median error in the temperature measurement for these stars (45 K) is lower than the median deviation to the fit, suggesting the potential for improvement. Iterating on the fit and removing outliers that lie further than 3σ gives an identical solution, but reduces the number of points used from 39 to 33. However, it does not improve the error of the fit by much. The scatter in the points with a $(B-V) > 0.6$ are clearly the cause of the ill-correlated relation, as illustrated in Figure 7.

5.1.2. $(V-K)$–T_{EFF}

We also present a fit of the temperature versus $(V-K)$ color index (Equation (9) and Figure 8), the benefit here being that $(V-K)$ colors are less sensitive to the stellar abundances than the $(B-V)$ colors. A solution including all stars gives a median deviation in temperature of 67 K, with only one extreme outlier, HD 162003 (+5.8 σ).[19] Omitting this star, we arrive at our final solution, practically identical from the first, with a median temperature deviation of 64 K. The statistical overview for this solution can be found in Table 11, and Figure 8 illustrates the fit. We note that the solution is identical when clipping stars that lie more than 3.5σ from the fit (instead of 5-σ) and has an improved median deviation in temperature of 56 K. As expected, the temperatures for the two previously mentioned metal-poor stars, HD 6582 and HD 103095, agree exceptionally well with the temperature–$(V-K)$ relation:

$$\begin{aligned}\log T_{\rm EFF} = {} & 3.9685 \pm 0.0034 + 0.0830 \pm 0.0570(V-K) \\ & - 1.8948 + 0.2874(V-K)^2 + 4.0799 \\ & \pm 0.5438(V-K)^3 - 3.7353 \pm 0.4739(V-K)^4 \\ & + 1.5651 \pm 0.1936(V-K)^5 - 0.2472 \\ & \pm 0.0301(V-K)^6 \quad \text{for } 0.0 < (V-K) < 2.0. \end{aligned} \quad (8)$$

[19] We note that this star has a visual companion HD 162004, and thus could have bad photometry. Note that HD 162003 was an outlier in the $B-V$ relation, with a negative offset from the fit derived.

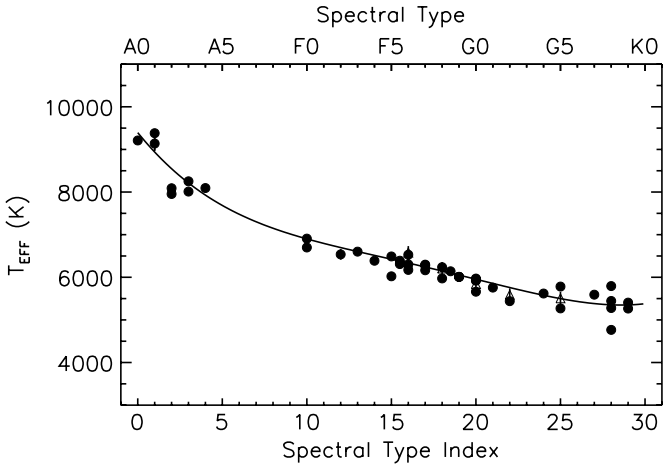

Figure 9. Data and solution for the temperature–spectral-type relation shown as circles and a solid line, respectively. The 1σ errors in temperature are shown, but are typically smaller than the data point. The data from Table 7 in van Belle & von Braun (2009) are displayed as open triangles. For details, see Section 5.1.3 and Equation (10).

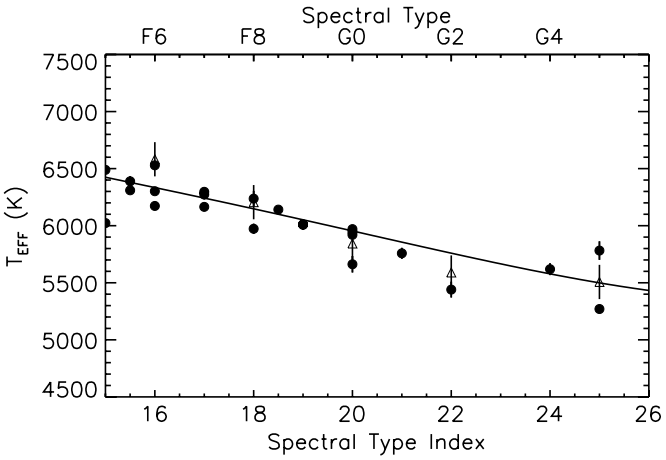

Figure 10. Zoomed-in version of Figure 9, showing the region that overlaps with the solution presented in van Belle & von Braun (2009). Our data and solution for the temperature–spectral-type relation are shown as circles and a solid line, respectively. The 1σ errors in temperature are shown, but are typically smaller than the data point. The data from Table 7 in van Belle & von Braun (2009) are displayed as open triangles. For details, see Section 5.1.3 and Equation (10).

5.1.3. Spectral-type–T_{EFF}

We next derive a useful (albeit less accurate) relation between spectral type and temperature. We do this by converting the spectral types for each star into a numerical value, following the scheme: A0, A1, A2 ... F0, F1, F2 ... G0, G1, G2, ..., K0 $\rightarrow$ 0, 1, 2, ..., 10, 11, 12, ..., 20, 21, 22, ..., 30. Again, we omit the two metal-poor stars previously mentioned and fit a fourth-order polynomial to arrive at the relation

$$T_{\rm EFF} = 9393.59 \pm 60.45 - 490.25 \pm 28.79{\rm ST} + 36.44 \pm 3.62{\rm ST}^2 - 1.44 \pm 0.17{\rm ST}^3 + 0.0208 \pm 0.0027{\rm ST}^4 \quad \text{for A0} < \text{ST} < \text{K0 and [Fe/H]} > -0.75, \tag{9}$$

where in this equation, the variable ST refers to the numerical value for the spectral-type index. The fit for Equation (10) has a median absolute deviation of 90 K and is plotted in Figure 9. In the range from F6 to G5, we also show the fit from the data in Table 7 from van Belle & von Braun (2009; Figure 10 is a close-up view of this range) and our results are consistent with each other.

5.2. Comparison to Indirectly Determined Temperatures

In the literature, three surveys exist of nearby stars that include objects that overlap with the majority of stars in this sample: Allende Prieto & Lambert (1999), Holmberg et al. (2007), and Takeda (2007). The number of stars in common with each survey respectively are 37, 34, and 25. We compare our results to these works in this section.

Allende Prieto & Lambert (1999, hereafter APL99) derive fundamental parameters for the stars in their survey by fitting model evolutionary tracks from Bertelli et al. (1994) to observed $(B-V)$ photometry and absolute V-band magnitude M_V. The Geneva–Copenhagen survey of the solar neighborhood II, done by Holmberg et al. (2007, hereafter GCS07), utilizes the Padova models (Girardi et al. 2000; Salasnich et al. 2000) to derive the stellar parameters based on Strömgren *uvby* calibrations to $T_{\rm EFF}$ and M_V. Last, Takeda (2007, hereafter Tak07) use the Yonsei–Yale (Y^2) stellar isochrones (Yi et al. 2001; Kim et al. 2002; Yi et al. 2003; Demarque et al. 2004) to fit their spectroscopically determined $T_{\rm EFF}$ along with the photometrically derived L (from the absolute magnitude and bolometric correction; see Takeda et al. 2005 for details). GCS07 demonstrate that these model isochrones (among others) show minimal differences when compared to each other, also seen in Boyajian et al. (2008). However, we choose to compare all three sources since the target overlap is not identical or complete with respect to our own, as well as the fact that different data sets and photometric indices were used for each group.

In Figure 11, we compare our temperatures to the temperatures of the stars in common in each reference. The most apparent discrepancies appear when comparing our results to those in APL99. For most cases seen here, APL99 overestimate the effective temperature of the star through the entire range of effective temperatures by about 5%, up to 15%. GCS07 and Tak07 are less drastic in comparison, but there is still a tendency of the models to overestimate the temperatures by a couple percent. Figures 12 and 13 plot the fractional offset of the stellar temperature from each method versus $(B-V)$ color index and metallicity. For the hottest/bluest of stars ($T_{\rm EFF} > 6500$, $B-V < 0.4$, a range mostly covered by APL99 only), a positive offset is seen for all but one measurement. Likewise, temperatures of stars with the lowest metallicity are also overestimated in each reference compared to the temperatures presented here, but no trend can be identified with the sparse quantity of data available in this range.

The stars with the largest offsets in the effective temperatures of GCS07 are HD 103095 (5.5%), HD 146233 (5.8%) and HD 162003 (6.4%). Interestingly enough, these stars also have high discrepancies between their SED diameter and the limb-darkened diameter measured with CHARA. However, stars such as HD 10780 and HD 109358 also have high deviation in the SED diameter versus the limb-darkened diameter measured by CHARA, but their agreement with the temperature from GCS07 is at the $\sim$1% level. It is interesting to note that the star HD 146233 (18 Sco), which was first identified by Porto de Mello & da Silva (1997) to be a solar twin, is one of these stars with a large offset in effective temperature.

The agreement in temperature with Tak07 is better than both the APL99 and GCS07 surveys, but there is still a preference to higher temperatures than what we measure. The largest outliers in temperature offsets compared to Tak07 are HD 103095 (6.6%)

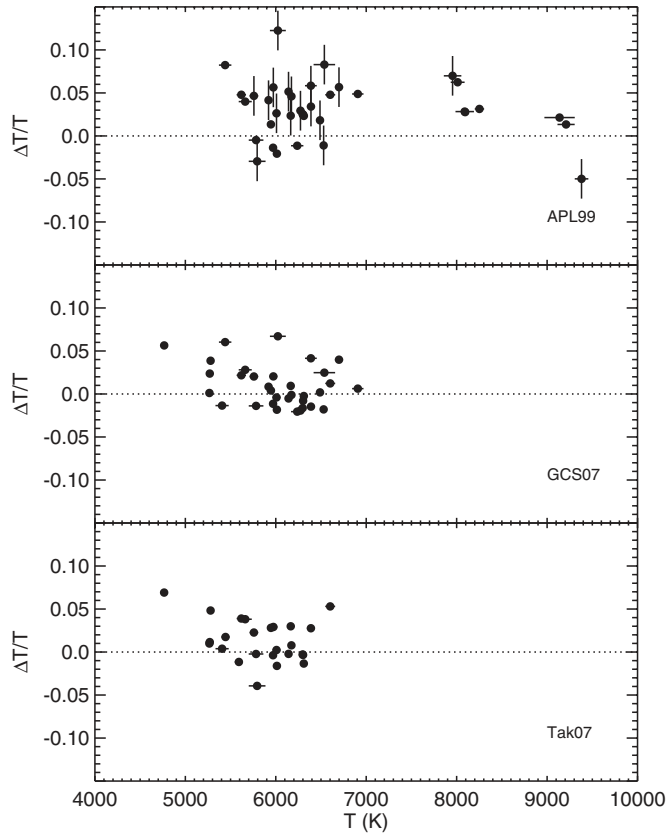

Figure 11. Data plotted show the dependence on the measured temperature vs. the fractional differences between model temperatures determined by Allende Prieto & Lambert (1999, APL99), Holmberg et al. (2007, GCS07), and Takeda (2007, Tak07) and the empirical values determined in this project, along with 1σ errors for each. The dotted line marks a zero deviation between each source.

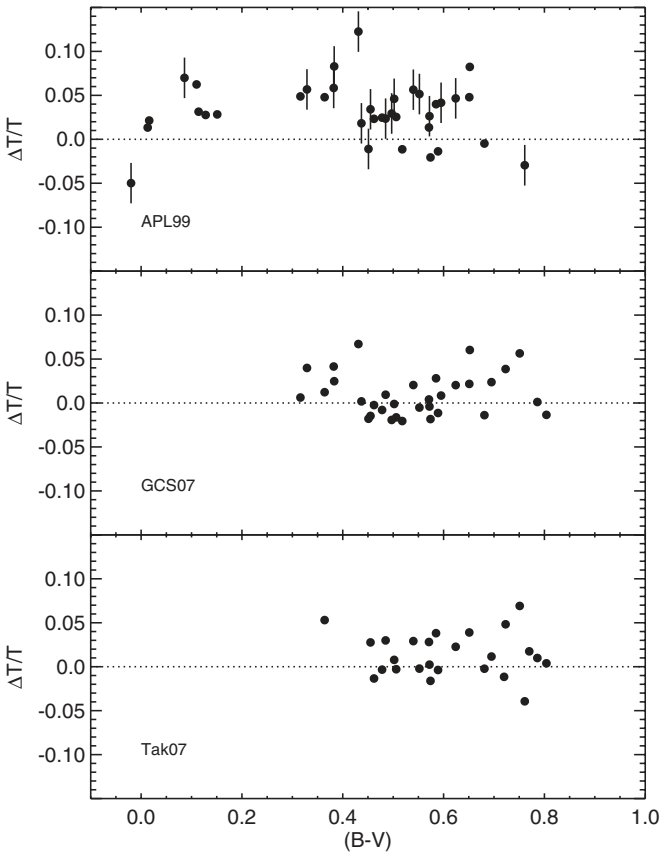

Figure 12. Data plotted show the dependence on the $(B-V)$ color index vs. the fractional differences between model temperatures determined by Allende Prieto & Lambert (1999, APL99), Holmberg et al. (2007, GCS07), and Takeda (2007, Tak07) and the empirical values determined in this project, along with 1σ errors for each. The dotted line marks a zero deviation between each source.

and HD 128167 (5.2%). Comparing these outliers to the GCS07 outliers, there are no two stars in each that show large deviations from the model versus CHARA temperature, with the exception of the very metal poor star, HD 103095. Again, it does not appear that a star's metallicity or color index is related to the deviation in temperatures of each source.

5.3. Isochrone Masses and Ages

We determine an estimate of the stellar mass and age by fitting our temperatures and luminosities presented in Section 4.2 to the Y^2 stellar isochrones (Yi et al. 2001; Kim et al. 2002; Yi et al. 2003; Demarque et al. 2004). We are able to do this for most stars observed for this work, but unfortunately, useful results are not obtainable when fitting isochrones to stars with $L < 0.75\,L_{\odot}$, because sensitivity to age in this region is minimal.[20] To run the model isochrones, input estimates are required for the abundance of iron [Fe/H] (Table 1) and α elements [α/Fe].[21] For each star, isochrones were generated in increments of 0.1 Gyr, in the range of 0.1–15 Gyr. We fit the model isochrones in the theoretical temperature–luminosity plane, where the solutions from the model are purely from the theory of stellar structure. This eliminates any dependence of the color table used in transforming the model isochrone temperature to observed photometric colors (Lejeune et al. 1998). Once a best-fit isochrone is established, an age along with the associated mass for this best-fit isochrone is recorded for each star. We show an example of this routine in Figure 14, and the results are listed in Table 12.

We calculate the errors on the best-fit isochrone mass and age using the 1σ temperature and luminosity maximum offset for the isochrone solution. It is worth noting that the metallicity input for the model isochrones has an impact on the derived age (and in turn also on the derived mass). Lower metallicity isochrones shift down and to the left on these diagrams, so for a star with a true metallicity less than the input value, a higher isochrone age would be found. The opposite is true for stars with higher values of metallicity, where a younger age would result. For our isochrone fits, we adopt fixed values of metallicity measured from a uniform source (in this case Holmberg et al. 2007) that are used in the model input for computations. Thus, relative ages may be correct while absolute ages are highly uncertain.[22]

5.4. Gravity Masses

With the linear radii known for all stars in the CHARA sample, we are able to determine the mass of a star using $\log g$ estimates published in APL99 and Tak07 using the relation

$$g_* = GM_*/R_*^2, \tag{10}$$

[20] Stars within this range are HD 6582, HD 10780, HD 101501, HD 103095, HD 131156, and HD 185144.

[21] The [α/Fe] for all stars are zero (Carney 1996). We assign [Fe/H] = 0 for HD 56537, HD 141795, and HD 213558 because no metallicity measurements are available in the literature for these stars.

[22] A characteristic error introduced by a 0.1 dex uncertainty in the metallicity may introduce errors ranging from about 0.1 to 2.0 Gyr and 0.06 $M_{\odot}$ for the A- to G-type stars, respectively.

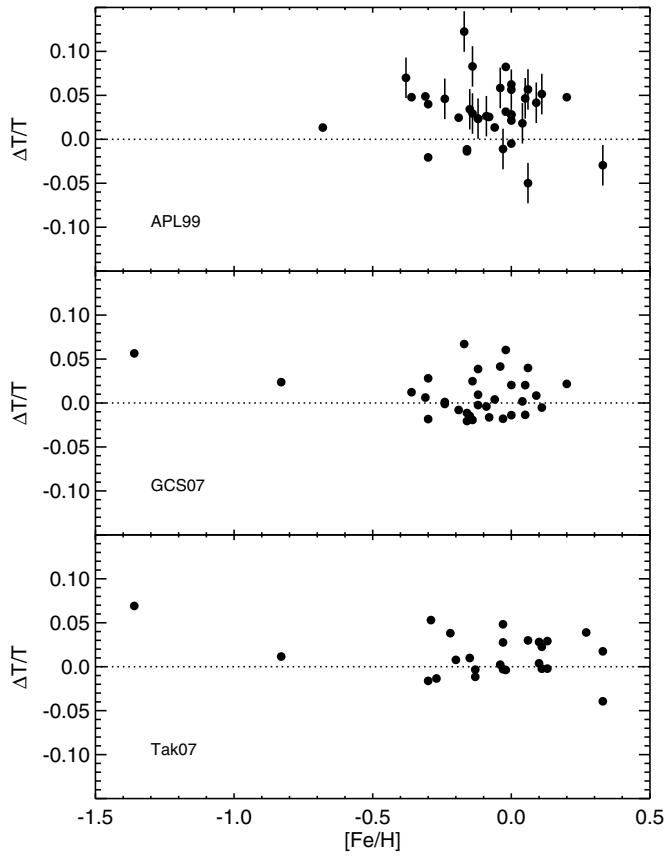

Figure 13. Data plotted show the dependence on the metallicity vs. the fractional differences between model temperatures determined by Allende Prieto & Lambert (1999, APL99), Holmberg et al. (2007, GCS07), and Takeda (2007, Tak07) and the empirical values determined in this project, along with 1σ errors for each. The dotted line marks a zero deviation between each source.

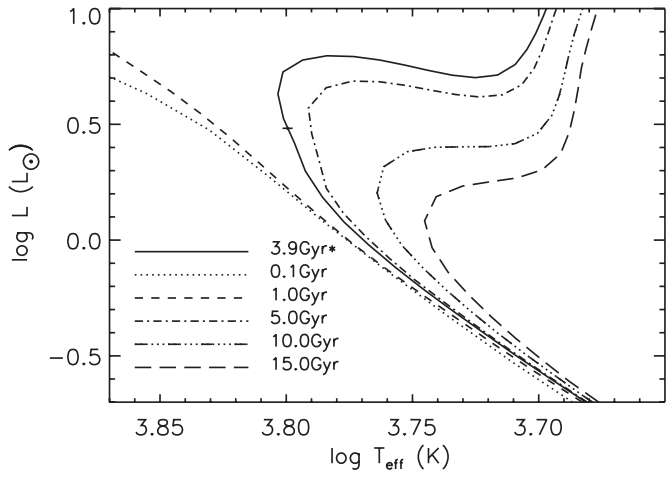

Figure 14. Stellar isochrones generated for HD 142860. The asterisk depicts best age fit to our data and is plotted as a solid line. The luminosity and temperature and the 1σ errors for this star are also plotted. These measurement errors show that the error in the x-direction (temperature) is the least constrained input for the isochrone fit.

where G is the gravitational constant, M_* is the mass of the star, R_* is the radius of the star, and g_* is the surface gravity of the star. Hereafter, we will refer to the mass derived in this manner as $M_{\rm g-R}$.

Table 12
Y^2 Model Isochrone Results for Stars with $L > 0.75\,L_\odot$

Star HD	Mass $\pm\sigma$ ($M_\odot$)	Age $\pm\sigma$ (Gyr)
4614	0.972 $\pm$ 0.012	5.4 $\pm$ 0.9
5015	1.182 $\pm$ 0.011	5.4 $\pm$ 0.3
16895	1.138 $\pm$ 0.010	4.0 $\pm$ 0.4
19373	1.169 $\pm$ 0.013	4.8 $\pm$ 0.5
20630	1.037 $\pm$ 0.042	0.2 $\pm$ 3.1
22484	1.139 $\pm$ 0.016	5.7 $\pm$ 0.4
30652	1.283 $\pm$ 0.006	1.3 $\pm$ 0.2
34411	1.041 $\pm$ 0.015	8.1 $\pm$ 0.8
39587	1.029 $\pm$ 0.029	2.0 $\pm$ 1.8
48737	1.706 $\pm$ 0.012	1.7 $\pm$ 0.1
56537	2.111 $\pm$ 0.010	0.8 $\pm$ 0.0
58946	1.355 $\pm$ 0.013	2.1 $\pm$ 0.2
81937	1.824 $\pm$ 0.016	1.4 $\pm$ 0.1
82328	1.506 $\pm$ 0.095	2.4 $\pm$ 0.7
82885	0.910 $\pm$ 0.020	10.6 $\pm$ 2.2
86728	1.034 $\pm$ 0.036	8.5 $\pm$ 1.8
90839	1.119 $\pm$ 0.035	1.5 $\pm$ 1.4
97603	2.061 $\pm$ 0.006	0.8 $\pm$ 0.0
102870	1.324 $\pm$ 0.005	3.3 $\pm$ 0.1
109358	0.852 $\pm$ 0.023	14.2 $\pm$ 2.1
114710	1.045 $\pm$ 0.013	4.6 $\pm$ 0.9
118098	1.940 $\pm$ 0.006	0.7 $\pm$ 0.0
126660	1.232 $\pm$ 0.058	4.2 $\pm$ 0.8
128167	1.194 $\pm$ 0.013	3.1 $\pm$ 0.4
141795	1.820 $\pm$ 0.026	0.5 $\pm$ 0.2
142860	1.184 $\pm$ 0.012	3.9 $\pm$ 0.3
146233	0.887 $\pm$ 0.019	14.9 $\pm$ 2.0
162003	1.311 $\pm$ 0.016	3.8 $\pm$ 0.1
164259	1.429 $\pm$ 0.013	2.4 $\pm$ 0.2
173667	1.422 $\pm$ 0.009	2.6 $\pm$ 0.1
177724	1.984 $\pm$ 0.006	0.8 $\pm$ 0.0
182572	1.186 $\pm$ 0.015	4.5 $\pm$ 0.8
185395	1.342 $\pm$ 0.011	2.8 $\pm$ 0.2
210418	1.858 $\pm$ 0.024	1.1 $\pm$ 0.1
213558	2.209 $\pm$ 0.037	0.4 $\pm$ 0.1
215648	1.192 $\pm$ 0.011	4.8 $\pm$ 0.2
222368	1.268 $\pm$ 0.009	3.4 $\pm$ 0.2

Notes. Isochrones are not sensitive to stars with $L < 0.75\,L_\odot$ which includes these stars in our survey: HD 6582, HD 10780, HD 101501, HD 103095, HD 131156, and HD 185144. Errors are calculated assuming the 1σ errors on temperature and luminosity. Refer to Section 5.3 for details.

5.5. Comparative Analysis

Masses derived from isochrone fitting ($M_{\rm Iso}$) and those obtainable when the surface gravity and radius are known through Equation (10) ($M_{\rm g-R}$) are compared in Figure 15 for the stars with gravity measurements published by APL99 and Tak07. There is significant scatter; however, we find that for stars greater than $\sim$1.3 $M_\odot$, the masses are overpredicted when using gravities from APL99. It is possible that the offset links back to the temperature offsets discussed in the previous section. For instance, if the model temperature used to fit the spectral lines to determine log g values for the stars is offset, this will in turn lead to spurious values of log g. Presumably, these overestimated temperatures will lead to a slightly more massive star because hotter stars on the main sequence are more massive than their cooler counterparts. Sure enough, this trend can be seen in Figure 16 when comparing the deviation in temperatures and masses for these stars. Ages derived are also affected in the sense that the stars will appear younger if their temperature or

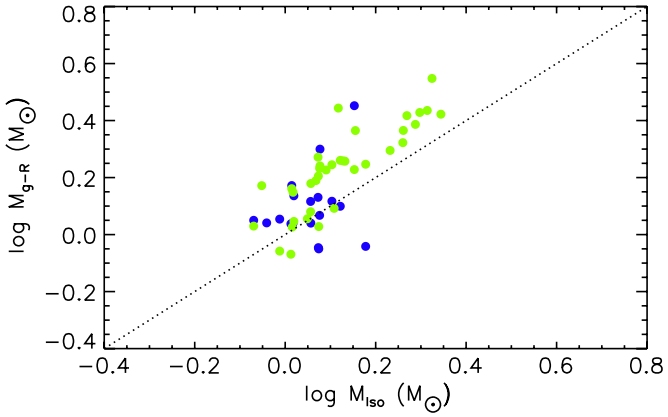

Figure 15. Masses derived from the Y^2 isochrones M_{Iso} compared to masses of stars calculated from the combination of log g estimates and our CHARA radii M_{g-R}. References for log g data for stars in common with the APL99 and Tak07 surveys are depicted in green and blue, respectively. The dotted line shows a 1:1 relation.

(A color version of this figure is available in the online journal.)

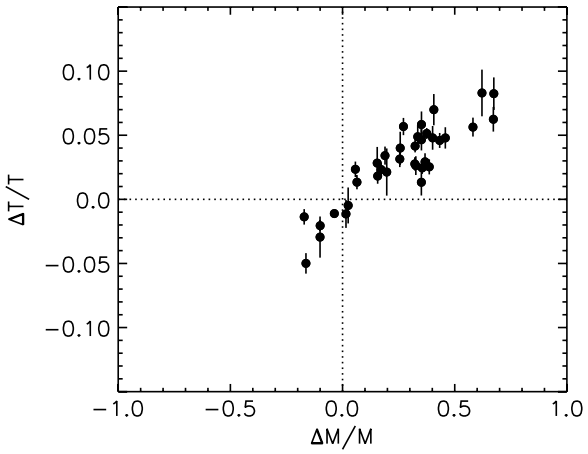

Figure 16. Fractional deviation of the masses derived from isochrone fitting and the ones derived when using APL99 log g in combination with CHARA radius measurements vs. the fractional offset of our measured temperature vs. the ones in APL99. The dotted lines indicate zero deviation.

log g is artificially offset to higher values. In fact, a slight trend may be seen in Figure 17 to support this when comparing our ages to the ages in GCS07 and Tak07 (APL99 did not publish ages), where our ages are typically greater.

The discussion in Holmberg et al. (2007) also gives several examples of how an offset in effective temperature will, in turn, offset the metallicity and argues that these effects double up when determining the ages of the stars, thereby producing false age–metallicity relations.

For further comparison, we introduce the data set presented in Andersen (1991). Andersen (1991) provides a compilation of data on all non-interacting eclipsing binaries (EB) known at the time—a total of 90 stars, most of which are on the main sequence. Section 4 in Andersen (1991) argues that the motivation for compiling the EB data is to aid in the prediction of single-star properties where masses and radii are unobtainable by direct measurements for a large number of stars. We use these data for eclipsing binaries to compare with our results for single stars in this section.

In Figure 18, we show the relation between $(B-V)$ color index and stellar mass. The mass–luminosity relation is shown in Figure 19. EB data from Andersen (1991) are plotted as

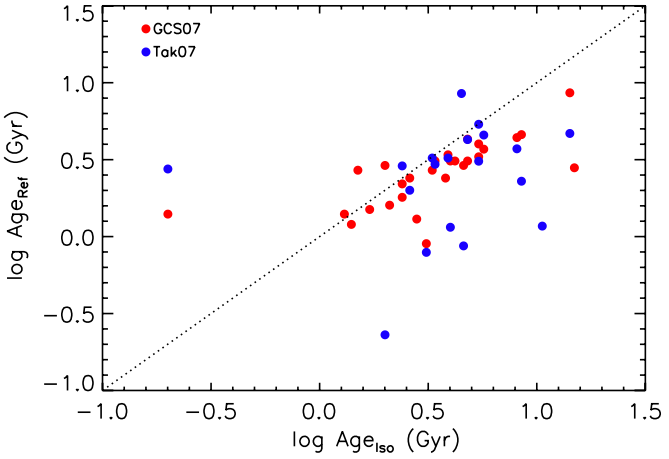

Figure 17. Ages derived from the Y^2 isochrones compared to ages of stars in common with GCS07 (red) and Tak07 (blue). The dotted line shows a 1:1 relation.

(A color version of this figure is available in the online journal.)

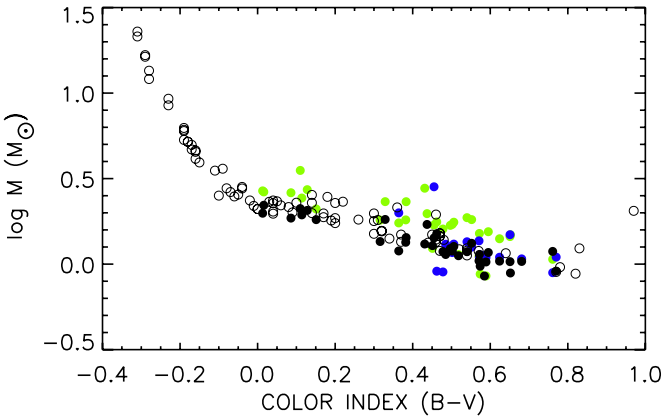

Figure 18. Mass vs. color index for eclipsing binaries (black open circles) plotted with masses derived from our sample using the Y^2 isochrones (black filled circles). Also plotted are the calculated M_{g-R} for stars in common with the APL99 (green filled circles), and Tak07 (blue filled circles) surveys.

(A color version of this figure is available in the online journal.)

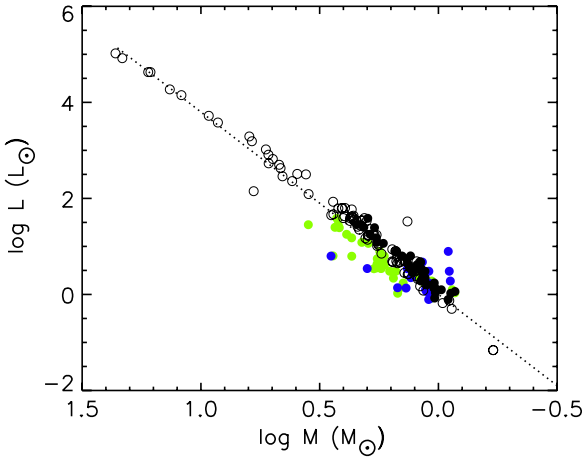

Figure 19. Mass vs. luminosity for eclipsing binaries (black open circles) plotted with masses derived from our sample using the Y^2 isochrones (black filled circles). Also plotted are the calculated M_{g-R} for stars in common with the APL99 (green filled circles) and Tak07 (blue filled circles) surveys. The dotted line is the relation $L \propto M^{3.8}$.

(A color version of this figure is available in the online journal.)

well as the masses for stars in this project derived from the Y^2 isochrones, and masses derived from the combination of the CHARA radii and log g estimates from each source (APL99 or Tak07).

The Y^2 masses we found are in excellent agreement with the sample of EB from Andersen (1991) with respect to $(B-V)$ color index and luminosity (Figures 18 and 19). However, comparing the M_{g-R} data points to the EB sample, we see that these masses are biased to larger masses, forcing them to appear underluminous compared to the EB sample as well as the Y^2 data points. The effect is again most apparent in the range where the APL99 gravities are used, where the systematics appear for stars with masses greater than $\sim 1.3\ M_{\odot}$.

6. SUMMARY AND CONCLUSION

In this paper, we present the angular diameters of nearby, main-sequence stars measured with the CHARA Array. The survey includes a total of 44 stars for which the angular diameter is measured to better than 4%. Robust bolometric flux measurements of the stars are presented, yielding absolute luminosities and effective temperatures measured to accuracies on the average of 1.8% and 1%, respectively. Lastly, we extract masses and ages of the stars by applying the Y^2 model isochrones to our data

We show that published values of such stellar parameters derived indirectly are not consistent with our results. Our data compared to the published values show that several sources overestimate the effective temperature by 1.5%–4%. The values for modeled stellar radius compensate this offset by being underestimated in order for the luminosity to come out right. Generally speaking, this offset is most apparent in the metal-poor stars as well as the earlier-type stars ($\gtrsim 1.3\ M_{\odot}$) that we observed. We propose that this preference for models to derive hotter temperatures is the cause for further divergence in a star's surface gravity measurements, which consequently yields higher masses and younger ages. Excellent agreement is seen when comparing our data to a large sample of EBs.

This data sample is used to solve for empirically based temperature relations for A-, F-, and G-type main-sequence stars, with precision close to the 1% level on the color–temperature calibrations. The results of the $B-V$ color–temperature relation are consistent with other relations for the stars redder than $B-V \sim 0.4$ (mid-F- through G-type). However, for stars earlier than this (the A- and early F-types), our solution is a couple hundred Kelvin cooler than all but one of the relations we use for comparison. This is likely due to the sparsity of good-quality empirical data used for fitting in this region. Our data is better correlated in the $V-K$ color–temperature relation than the interferometric data in van Belle & von Braun (2009) for the F- and G-type stars, due to the high precision of our measurements compared to theirs, but the fits to the data are indistinguishable in this range. For the earlier-type stars, moderate disagreement is still present, again from lack of complete sampling in this region.

Ongoing observations of more nearby main-sequence stars are under way by our group at the CHARA Array. Color–temperature calibrations with various other color indices will be implemented in the forthcoming papers in the series. Stellar metallicity was ignored in this work; however, including it in temperature relations will almost certainly beat the errors down even more than what we have achieved with the current fit. In our future efforts, we aim to populate the data set enough to identify accurate color–temperature–metallicity relations as well as extend the sample down to the lower end of the main sequence.

T.S.B. acknowledges support provided by NASA through Hubble Fellowship grant No. HST-HF-51252.01 awarded by the Space Telescope Science Institute, which is operated by the Association of Universities for Research in Astronomy, Inc., for NASA, under contract NAS 5-26555. The CHARA Array is funded by the National Science Foundation through NSF grant AST-0908253 and by Georgia State University through the College of Arts and Sciences. This research has made use of the SIMBAD literature database, operated at CDS, Strasbourg, France, and of NASA's Astrophysics Data System. This publication makes use of data products from the Two Micron All Sky Survey, which is a joint project of the University of Massachusetts and the Infrared Processing and Analysis Center/California Institute of Technology, funded by NASA and NSF.

REFERENCES

Absil, O., di Folco, E., Mérand, A., et al. 2008, A&A, 487, 1041
Abt, H. A., & Levy, S. G. 1976, ApJS, 30, 273
Allen, D. A., & Cragg, T. A. 1983, MNRAS, 203, 777
Allende Prieto, C., & Lambert, D. L. 1999, A&A, 352, 555
Alonso, A., Arribas, S., & Martinez-Roger, C. 1994, A&AS, 107, 365
Andersen, J. 1991, A&AR, 3, 91
Argue, A. N. 1963, MNRAS, 125, 557
Argue, A. N. 1966, MNRAS, 133, 475
Arp, H. C. 1958, AJ, 63, 118
Arribas, S., & Martinez Roger, C. 1987, A&AS, 70, 303
Arribas, S., & Martinez Roger, C. 1989, A&A, 215, 305
Aumann, H. H., & Probst, R. G. 1991, ApJ, 368, 264
Baines, E. K., McAlister, H. A., ten Brummelaar, T. A., et al. 2008, ApJ, 680, 728
Barnes, T. G., Evans, D. S., & Moffett, T. J. 1978, MNRAS, 183, 285
Barry, D. C. 1969, PASP, 81, 339
Baruch, J. E. F., Griffiths, W. K., Nittmann, J., et al. 1983, MNRAS, 202, 691
Behr, B. B., Hajian, A. R., Cenko, A. T., et al. 2009, ApJ, 705, 543
Bergeat, J., & Lunel, M. 1980, A&A, 87, 139
Berger, D. H., Gies, D. R., McAlister, H. A., et al. 2006, ApJ, 644, 475
Berriman, G., de Campli, W. M., Werner, M. W., & Hatchett, S. P. 1983, MNRAS, 205, 859
Bertelli, G., Bressan, A., Chiosi, C., Fagotto, F., & Nasi, E. 1994, A&AS, 106, 275
Blackwell, D. E., Petford, A. D., Arribas, S., Haddock, D. J., & Selby, M. J. 1990, A&A, 232, 396
Blackwell, D. E., & Shallis, M. J. 1977, MNRAS, 180, 177
Blackwell, D. E., Shallis, M. J., & Selby, M. J. 1979, MNRAS, 188, 847
Bok, B. J., Bok, P. F., & Miller, E. W. 1972, AJ, 77, 733
Bond, H. E. 1970, ApJS, 22, 117
Booth, A. J. 1997, in IAU Symp. 189, ed. T. R. Bedding, A. J. Booth, & J. Davis (Cambridge: Cambridge Univ. Press), 147
Bouigue, R. 1959, Ann. Obs. Astron. Meteo. Toulouse, 27, 47
Bowsher, E. C., McAlister, H. A., & Ten Brummelaar, T. A. 2010, Proc. SPIE, 7734, 92
Boyajian, T. S., McAlister, H. A., Baines, E. K., et al. 2008, ApJ, 683, 424
Boyajian, T. S., McAlister, H. A., Cantrell, J. R., et al. 2009, ApJ, 691, 1243
Breger, M. 1974, ApJ, 188, 53
Caillault, J.-P., & Patterson, J. 1990, AJ, 100, 825
Cameron, R. C. 1966, Georgetown Obs. Monogram, 21, 0
Campins, H., Rieke, G. H., & Lebofsky, M. J. 1985, AJ, 90, 896
Cardelli, J. A., Clayton, G. C., & Mathis, J. S. 1989, ApJ, 345, 245
Carney, B. W. 1996, PASP, 108, 900
Carney, B. W. 1979, ApJ, 233, 211
Carney, B. W. 1983a, AJ, 88, 623
Carney, B. W. 1983b, AJ, 88, 610
Carney, B. W., & Aaronson, M. 1979, AJ, 84, 867
Carter, B. S. 1990, MNRAS, 242, 1
Casagrande, L., Ramírez, I., Meléndez, J., Bessell, M., & Asplund, M. 2010, A&A, 512, A54

Celis, S. L. 1975, A&AS, 22, 9
Claret, A. 2000, A&A, 363, 1081
Code, A. D., Bless, R. C., Davis, J., & Brown, R. H. 1976, ApJ, 203, 417
Cohen, M., Wheaton, W. A., & Megeath, S. T. 2003, AJ, 126, 1090
Colina, L., Bohlin, R., & Castelli, F. 1996, AJ, 112, 307
Cousins, A. W. J. 1963, Mon. Notes Astron. Soc. South. Afr., 22, 12
Cousins, A. W. J. 1964, Mon. Notes Astron. Soc. South. Afr., 23, 175
Cousins, A. W. J. 1984, S. Afr. Astron. Obs. Circ., 8, 59
Cousins, A. W. J., & Stoy, R. H. 1962, R. Greenwich Obs. Bull., 64, 103
Cowley, A. P., Hiltner, W. A., & Witt, A. N. 1967, AJ, 72, 1334
Cox, A. N. (ed.) 2000, Allen's Astrophysical Quantities (4th ed.; New York: AIP)
Crawford, D. L. 1975, AJ, 80, 955
Crawford, D. L., & Barnes, J. V. 1969, AJ, 74, 407
Crawford, D. L., & Barnes, J. V. 1970, AJ, 75, 978
Crawford, D. L., Barnes, J. V., Faure, B. Q., & Golson, J. C. 1966, AJ, 71, 709
Crawford, D. L., Barnes, J. V., Gibson, J., et al. 1972, A&AS, 5, 109
Crawford, D. L., & Perry, C. L. 1989, PASP, 101, 601
Cutri, R. M., Skrutskie, M. F., van Dyk, S., et al. 2003, The 2MASS All Sky Catalog of Point Sources (Pasadena, CA: IPAC)
Danziger, I. J., & Dickens, R. J. 1967, ApJ, 149, 55
Davis, J. 1985, in IAU Symp. 111, Calibration of Fundamental Stellar Quantities, ed. D. S. Hayes, L. E. Pasinetti, & A. G. D. Philip (Cambridge: Cambridge Univ. Press), 193
Davis, J. 1997, in IAU Symp. 189, Fundamental Stellar Properties: The Interaction between Observation and Theory, ed. T. R. Bedding, A. J. Booth, & J. Davis (Cambridge: Cambridge Univ. Press), 31
Demarque, P., Woo, J.-H., Kim, Y.-C., & Yi, S. K. 2004, ApJS, 155, 667
de Vaucouleurs, G. 1959, Planet. Space Sci., 2, 26
Dyck, H. M., Benson, J. A., van Belle, G. T., & Ridgway, S. T. 1996, AJ, 111, 1705
Elias, J. H., Frogel, J. A., Matthews, K., & Neugebauer, G. 1982, AJ, 87, 1029
Elliott, J. E. 1974, AJ, 79, 1082
Fabregat, J., & Reglero, V. 1990, A&AS, 82, 531
Feinstein, A. 1974, AJ, 79, 1290
Fernie, J. D. 1969, J. R. Astron. Soc. Can., 63, 133
Fernie, J. D., Hagen, J. P., Jr., Hagen, G. L., & McClure, L. 1971, PASP, 83, 79
Fitch, W. S. 1955, ApJ, 121, 690
Frank, J., King, A. R., Sherrington, M. R., Jameson, R. F., & Axon, D. J. 1981, MNRAS, 195, 505
Frogel, J. A., Persson, S. E., Matthews, K., & Aaronson, M. 1978, ApJ, 220, 75
Gascoigne, S. C. B. 1962, MNRAS, 124, 201
Gehrz, R. D., & Woolf, N. J. 1970, ApJ, 161, L213
Ghosh, S. K., Iyengar, K. V. K., Tandon, S. N., et al. 1984, MNRAS, 206, 611
Girardi, L., Bressan, A., Bertelli, G., & Chiosi, C. 2000, A&AS, 141, 371
Glass, I. S. 1974, Mon. Notes Astron. Soc. South. Afr., 33, 53
Glass, I. S. 1975, MNRAS, 171, 19P
Grant, G. 1959, ApJ, 129, 62
Gray, D. F. (ed.) 1992, The Observation and Analysis of Stellar Photospheres (Cambridge: Cambridge Univ. Press), 470
Gray, R. O. 1998, AJ, 116, 482
Gray, R. O., Corbally, C. J., Garrison, R. F., McFadden, M. T., & Robinson, P. E. 2003, AJ, 126, 2048
Gray, R. O., Corbally, C. J., Garrison, R. F., et al. 2006, AJ, 132, 161
Gray, R. O., Napier, M. G., & Winkler, L. I. 2001, AJ, 121, 2148
Gray, R. O., & Olsen, E. H. 1991, A&AS, 87, 541
Grønbech, B., & Olsen, E. H. 1976, A&AS, 25, 213
Grønbech, B., Olsen, E. H., & Strömgren, B. 1976, A&AS, 26, 155
Guetter, H. H. 1977, AJ, 82, 598
Guetter, H. H. 1979, AJ, 84, 1846
Gutierrez-Moreno, A., & Moreno, H. 1968, ApJS, 15, 459
Gutierrez-Moreno, A., et al. 1966, Publ. Dept. Astron. Univ. Chile, 1, 1
Haas, M., & Leinert, C. 1990, A&A, 230, 87
Häggkvist, L., & Oja, T. 1966, Ark. Astron., 4, 137
Häggkvist, L., & Oja, T. 1969, Ark. Astron., 5, 303
Haggkvist, L., & Oja, T. 1970, private communication
Han, I., & Gatewood, G. 2002, PASP, 114, 224
Hanbury Brown, R., Davis, J., & Allen, L. R. 1974a, MNRAS, 167, 121
Hanbury Brown, R. H., Davis, J., Lake, R. J. W., & Thompson, R. J. 1974b, MNRAS, 167, 475
Harris, D. L., III, & Upgren, A. R. 1964, ApJ, 140, 151
Hauck, B., & Mermilliod, M. 1998, A&AS, 129, 431
Henry, J. P., Becklin, E. E., & Telesco, C. M. 1984, ApJ, 280, 98
Hoffleit, D., & Jaschek, C. (ed.) 1991, The Bright Star Catalogue (New Haven, CT: Yale Univ. Observatory)
Hogg, A. R. 1958, Mount Stromlo Obs. Mimeographs, 2, 1
Holmberg, J., Nordström, B., & Andersen, J. 2007, A&A, 475, 519
Holmberg, J., Nordström, B., & Andersen, J. 2008, A&A, 501, 941
Imagawa, F. 1967, Mem. Coll. Sci. Kyoto Imp. Univ., 31, 93
Iriarte, B., Johnson, H. L., Mitchell, R. I., & Wisniewski, W. K. 1965, S&T, 30, 21
Irvine, W. M., Simon, T., Menzel, D. H., Pikoos, C., & Young, A. T. 1968a, AJ, 73, 807
Irvine, W. M., Simon, T., Menzel, D. H., et al. 1968b, AJ, 73, 251
Irwin, J. B. 1961, ApJS, 6, 253
Jennens, P. A., & Helfer, H. L. 1975, MNRAS, 172, 667
Jerzykiewicz, M., & Serkowski, K. 1966, PASP, 78, 546
Johansen, K. T., & Gyldenkerne, K. 1970, A&AS, 1, 165
Johnson, H. L. 1953, ApJ, 117, 361
Johnson, H. L. 1964, Bol. Obs. Tonantzintla Tacubaya, 3, 305
Johnson, H. L. 1965a, ApJ, 141, 170
Johnson, H. L. 1965b, Commun. Lunar Planet. Lab., 3, 73
Johnson, H. L. 1968, in Interstellar Extinction, ed. B. M. Middlehurst & L. H. Aller (Chicago, IL: Univ. Chicago Press), 167
Johnson, H. L., & Harris, D. L. 1954, ApJ, 120, 196
Johnson, H. L., & Knuckles, C. F. 1957, ApJ, 126, 113
Johnson, H. L., MacArthur, J. W., & Mitchell, R. I. 1968, ApJ, 152, 465
Johnson, H. L., Mitchell, R. I., Iriarte, B., & Wisniewski, W. Z. 1966, Commun. Lunar Planet. Lab., 4, 99
Johnson, H. L., & Morgan, W. W. 1953, ApJ, 117, 313
Jones, R. V., Carney, B. W., & Latham, D. W. 1988, ApJ, 332, 206
Kenyon, S. J. 1988, AJ, 96, 337
Kenyon, S. J., & Gallagher, J. S. 1983, AJ, 88, 666
Kilkenny, D., & Menzies, J. W. 1986, MNRAS, 222, 373
Kim, Y.-C., Demarque, P., Yi, S. K., & Alexander, D. R. 2002, ApJS, 143, 499
Konacki, M. 2005, ApJ, 626, 431
Kostjuk, N. D. 2004, VizieR Online Data Catalog, 4027, 0
Kozok, J. R. 1985, A&AS, 61, 387
Lake, R. 1962, Mon. Notes Astron. Soc. South. Afr., 21, 191
Lake, R. 1964, Mon. Notes Astron. Soc. South. Afr., 23, 14
Leggett, S. K., Bartholomew, M., Mountain, C. M., & Selby, M. J. 1986, MNRAS, 223, 443
Leitherer, C., Hefele, H., Stahl, O., & Wolf, B. 1982, A&A, 108, 102
Leitherer, C., & Wolf, B. 1984, A&A, 132, 151
Lejeune, T., Cuisinier, F., & Buser, R. 1998, A&AS, 130, 65
Little-Marenin, I. R., Simon, T., Ayres, T. R., et al. 1986, ApJ, 303, 780
Ljunggren, B., & Oja, T. 1965, Ark. Astron., 3, 439
Lonsdale, C. J., Becklin, E. E., Lee, T. J., & Stewart, J. M. 1982, AJ, 87, 1819
Lutz, T. E. 1971, PASP, 83, 488
Markwardt, C. B. 2009, in ASP Conf. Ser. 411, Astronomical Data Analysis Software and Systems XVIII, ed. D. A. Bohlender, D. Durand, & P. Dowler (San Francisco, CA: ASP), 251
Marlborough, J. M. 1964, AJ, 69, 215
McCarthy, D. W., Jr. 1984, AJ, 89, 433
McClure, R. D. 1970, AJ, 75, 41
Mechler, G. E. 1976, AJ, 81, 107
Mechler, G. E., & McGinnis, S. K. 1978, AJ, 83, 1646
Mendoza, E. E., Gomez, V. T., & Gonzalez, S. 1978, AJ, 83, 606
Mendoza, E. E., & Gonzalez, S. F. 1974, RevMexAA, 1, 67
Mermilliod, J.-C. 1986, Catalogue of Eggen's UBV Data, 0
Mermilliod, J. C. 1997, VizieR Online Data Catalog, 2168, 0
Miczaika, G. R. 1954, AJ, 59, 233
Mitchell, R. I., & Schuster, W. J. 1985, AJ, 90, 2116
Moffett, T. J., & Barnes, T. G., III. 1979, PASP, 91, 180
Morbey, C. L., & Griffin, R. F. 1987, ApJ, 317, 343
Moreno, H. 1971, A&A, 12, 442
Nakagiri, M., & Yamashita, Y. 1979, Ann. Tokyo Astron. Obs., 17, 221
Naur, P. 1955, ApJ, 122, 182
Neckel, H. 1974, A&AS, 18, 169
Neugebauer, G., & Leighton, R. B. 1969, Two-micron Sky Survey: A Preliminary Catalogue (Washington, DC: NASA)
Nicolet, B. 1978, A&AS, 34, 1
Niconov, V. B., Nekrasova, S. V., Polosuina, N. S., Rachkouvsky, N. D., & Chuvajev, W. K. 1957, Izv. Ordena Trudovogo Krasnogo Znameni Krym. Astrofiz. Obs., 17, 42
Nidever, D. L., Marcy, G. W., Butler, R. P., Fischer, D. A., & Vogt, S. S. 2002, ApJS, 141, 503
Nikrasova, V., Nikonov, V. B., Polosukhina, N. S., & Rybka, E. 1962, Izv. Ordena Trudovogo Krasnogo Znameni Krym. Astrofiz. Obs., 27, 228
O'Connell, D. J. K. 1964, Ric. Astron., 6, 523
Oja, T. 1963, Ark. Astron., 3, 273
Oja, T. 1970, private communication
Oja, T. 1983, A&AS, 52, 131
Oja, T. 1984, A&AS, 57, 357

Oja, T. 1985a, A&AS, 61, 331
Oja, T. 1985b, A&AS, 59, 461
Oja, T. 1986, A&AS, 65, 405
Olsen, E. H. 1977, A&AS, 29, 313
Olsen, E. H. 1983, A&AS, 54, 55
Olsen, E. H. 1993, A&AS, 102, 89
Olsen, E. H. 1994a, A&AS, 104, 429
Olsen, E. H. 1994b, A&AS, 106, 257
Olson, E. C. 1974, AJ, 79, 1424
Penston, M. J. 1973, MNRAS, 164, 133
Perry, C. L. 1969, AJ, 74, 139
Pfleiderer, J., Dachs, J., & Haug, U. 1966, Z. Astrophys., 64, 116
Philip, A. G. D., & Philip, K. D. 1973, ApJ, 179, 855
Pickles, A. J. 1998, PASP, 110, 863
Piirola, V. 1976, Observatory and Astrophysics Laboratory University of Helsinki Report, 1, 0
Porto de Mello, G. F., & da Silva, L. 1997, ApJ, 482, L89
Rakos, K. D., Albrecht, R., Jenkner, H., et al. 1982, A&AS, 47, 221
Reglero, V., & Fabregat, J. 1991, A&AS, 90, 25
Reglero, V., Gimenez, A., de Castro, E., & Fernandez-Figueroa, M. J. 1987, A&AS, 71, 421
Richichi, A., Percheron, I., & Khristoforova, M. 2005, A&A, 431, 773
Roman, N. G. 1955, ApJS, 2, 195
Royer, F., Zorec, J., & Gomez, A. E. 2006, VizieR Online Data Catalog, 346, 30671
Rucinski, S. M. 1983, IBVS, 2277, 1
Rufener, F. 1976, A&AS, 26, 275
Sadler, D. H. (ed.) 1961, XIth General Assembly—Transactions of the IAU Vol. XI B (Berkeley, CA: IAU)
Salasnich, B., Girardi, L., Weiss, A., & Chiosi, C. 2000, A&A, 361, 1023
Sanwal, N. B., Parthasarathy, M., & Abhyankar, K. D. 1973, Observatory, 93, 30
Schild, R. E. 1973, AJ, 78, 37
Schmidt, E. G. 1971, ApJ, 165, 335
Schuster, W. J., & Nissen, P. E. 1988, A&AS, 73, 225
Selby, M. J., Hepburn, I., Blackwell, D. E., et al. 1988, A&AS, 74, 127
Serkowski, K. 1961, Lowell Obs. Bull., 5, 157
Shao, C. Y. 1964, AJ, 69, 858
Sharpless, S. 1952, ApJ, 116, 251
Sjögren, U. 1964, Ark. Astron., 3, 339
Sowell, J. R., & Wilson, J. W. 1993, PASP, 105, 36
Stetson, P. B. 1991, AJ, 102, 589
Stokes, N. R. 1972a, MNRAS, 159, 165
Stokes, N. R. 1972b, MNRAS, 160, 155
Szabados, L. 1981, Commun. Konkoly Obs. Hungary, 77, 1
Takeda, Y. 2007, PASJ, 59, 335
Takeda, Y., Ohkubo, M., Sato, B., Kambe, E., & Sadakane, K. 2005, PASJ, 57, 27
Taylor, B. J., & Joner, M. D. 1992, PASP, 104, 911
Telesco, C. M., Decher, R., & Gatley, I. 1985, ApJ, 299, 896
Telesco, C. M., Decher, R., & Gatley, I. 1986, ApJ, 302, 632
Telesco, C. M., & Gatley, I. 1984, ApJ, 284, 557
ten Brummelaar, T. A., McAlister, H. A., Ridgway, S. T., et al. 2005, ApJ, 628, 453
Tifft, W. G. 1963, MNRAS, 125, 199
Tolbert, C. R. 1964, ApJ, 139, 1105
Toyota, E., Itoh, Y., Ishiguma, S., et al. 2009, PASJ, 61, 19
van Belle, G. T., Creech-Eakman, M. J., & Hart, A. 2009, MNRAS, 394, 1925
van Belle, G. T., Lane, B. F., Thompson, R. R., et al. 1999, AJ, 117, 521
van Belle, G. T., & van Belle, G. 2005, PASP, 117, 1263
van Belle, G. T., van Belle, G., Creech-Eakman, M. J., et al. 2008, ApJS, 176, 276
van Belle, G. T., & von Braun, K. 2009, ApJ, 694, 1085
van den Bergh, S. 1967, AJ, 72, 70
van Leeuwen, F. 2007, in Hipparcos, the New Reduction of the Raw Data, ed. F. van Leeuwen (Astrophysics and Space Science Library, Vol. 350; Dordrecht: Springer), 20
Veeder, G. J. 1974, AJ, 79, 1056
Veeder, G. J., Matson, D. L., & Smith, J. C. 1978, AJ, 83, 651
Voelcker, K. 1975, A&AS, 22, 1
Wallerstein, G., & Helfer, H. L. 1961, ApJ, 133, 562
Warren, W. H., Jr. 1973, AJ, 78, 192
Warren, W. H., Jr., & Hesser, J. E. 1977, ApJS, 34, 115
Wenger, M., Ochsenbein, F., Egret, D., et al. 2000, A&AS, 143, 9
Yi, S., Demarque, P., Kim, Y.-C., et al. 2001, ApJS, 136, 417
Yi, S. K., Kim, Y.-C., & Demarque, P. 2003, ApJS, 144, 259
Zhao, M., Monnier, J. D., Pedretti, E., et al. 2009, ApJ, 701, 209